CHALMERS

# Development of a Control Strategy for a Percussive Drill driven by a Tubular Linear PMSM

*Master of Science Thesis*


Jimmy Björkman
Anton Klintberg

Department of Energy & Environment
Division of Electric Power Engineering
Chalmers University of Technology
Göteborg, Sweden, 2014

# Development of a Control Strategy for a Percussive Drill driven by a Tubular Linear PMSM

*Master of Science Thesis in the Master Program in Electric Power Engineering*

Jimmy Björkman
Anton Klintberg

Department of Energy & Environment
Division of Electric Power Engineering
CHALMERS UNIVERSITY OF TECHNOLOGY
Göteborg, Sweden, 2014

Development of a Control Strategy for a Percussive Drill driven by a Tubular Linear PMSM



Department of Energy & Environment
*Division of Electric Power Engineering*
Chalmers University of Technology
SE-412 96 Göteborg
Sweden

Tel. +46-(0)31 772 1000

Department of Energy and Environment
Göteborg, Sweden, 2014

Development of a Control Strategy for a Percussive Drill driven by a Tubular Linear PMSM
Master of Science Thesis in the Master Program in Electric Power Engineering
JIMMY BJÖRKMAN
ANTON KLINTBERG
Department of Energy and Environment
Division of Electric Power Engineering
Chalmers University of Technology

## Abstract

This thesis presents a control strategy for a percussive drill driven by an oscillating Tubular Linear Permanent Magnet Synchronous Machine (TLPMSM). The drill consists of a piston with permanent magnets and a casing with integrated stator windings. The casing encapsulate the whole unit and should be used to hammer into rocks. Between the piston and the casing there are two gas springs used to store the kinetic energy of the masses as potential energy while the oscillating masses change direction.

The electric force from the TLPMSM should be used to bring the mechanical system in resonance. When the system is in resonance only a small amount of electric energy is needed to maintain the oscillation. The electric energy injected is needed to compensate for the losses in the system and the energy lost when the casing hits the rock.

The developed control strategy consists of a field oriented vector controller for the current and an outer controller for the mechanical oscillations. The outer controller is a proportional controller with positive feedback, which is found to have particularly good properties for the application. The outer controller controls the oscillation at the resonance frequency without any information about the process. This is highly desirable since it is very challenging to make an accurate model of a rock. Furthermore, the controller only demands a current when the the back emf is non zero. This means that when the TLPMSM is unable to produce any output power the current in the windings is zero, which prevents unnecessary copper losses. It is shown that the relative position between piston and casing oscillates twice for each time the casing strikes the rock surface. In the simulated scenario, the impact force from the casing to the rock can reach 645 kN with an oscillation frequency of 38 Hz. To increase the oscillation frequency the gas spring pressure need to be increased.

Two methods to make the control strategy sensorless are also presented. The first strategy is a Statically Compensated Voltage Model (SCVM) which is based on the information provided by the induced back emf. The second strategy is based on saliency in the machine and uses injection of a high frequency square wave signal. In this work this strategy is referred to as Square Wave Injection. Both techniques are working in the application but they have different advantages and disadvantages. It is shown that the SCVM is insensitive to measurement noise since 10 % noise could be added to the current measurement without any trouble. It is also shown that it is dependent on good parameter estimation, especially for the rotor flux. An error in the parameter estimations leads to a lowering of the impact force from the casing to the rock from 417 kN per hit to 343 kN per hit.

For Square wave injection it is the opposite. It is sensitive to measurement noise since only 0.2 % current measurement noise could be added without that the estimation stopped working. If the oscillation frequency is increased the noise level need to be even lower. However, it is not dependent on parameter estimations since process parameters are almost not used.

When each estimation techniques is simulated without measurement noise the square wave injection technique gives a lower maximum position estimaton error than the SCVM, 0.82 mm versus 1.64 mm. But for the square wave injection technique the position estimation error is high at the instant when the current is applied. Since the force generating current is erronously applied an impact force from the casing to rock of 364 kN is reached and this is lower compared to the impact force of 417 kN when the SCVM is used.

It is recommended to use SCVM for this application. The SCVM can be used in a larger range of oscillation frequencies for the mechanical system and is more robust against non-ideal conditions.

**Index terms:** Tubular Linear PMSM, percussive drilling, sensorless current control, signal injection, SCVM.

**Acknowledgements**

We would like to thank Resonator AS and particularly Ravindra Babu Ummaneni and André Dahl-Jacobsen for giving us the opportunity to perform our master thesis and for their friendly attitude during our visits.

We would also like to thank our examiner Dr. Stefan Lundberg for providing us with the idea of using positive feedback in the control loop and for other valuable input during the project.

Jimmy Björkman and Anton Klintberg
Göteborg, Sweden, May 2014

# Nomenclature

In Table 1 and Table 2 the abbreviations and subscripts used throughout the report are presented. In Table 3 all symbols and variables are shown. In Table 4 the parameters of the TLPMSM used in the project are presented.

**Table 1:** Abbreviations

| Abbreviation | Explanation |
|---|---|
| TLPMSM | Tubular Linear Permanent Magnet Synchronous Machine |
| PWM | Pulse Width Modulation |
| PLL | Phase Locked Loop |
| ROP | Rate of Penetration |
| SCVM | Statically Compensated Voltage Model |

**Table 2:** Superscripts

| Superscript | Explanation |
|---|---|
| $^r$ | Rotor reference frame |
| $^s$ | Stator reference frame |
| $\hat{}$ | Estimated value |

**Table 3:** Symbols and variables

| Symbols and variables | Explanation |
|---|---|
| $u_a$, $u_b$, $u_c$ | Phase voltages [V] |
| U | Voltage amplitude [V] |
| i | Current [A] |
| $\omega$ | Relative angular speed between rotor and stator [rad/s] |
| v | Relative speed between rotor and stator [m/s] |
| x | Relative position between rotor and stator [m] |
| $x_p$ | Position of piston [m] |
| $x_c$ | Position of casing [m] |
| $\theta$ | Electrical angle [rad] |
| $F_e$ | Electromechanical force [N] |
| $F_{WOB}$ | Force on top of the resonator [N] |
| $f_{rock}$ | Force from rock [N] |
| $f_{gas}$ | Force from gas springs [N] |
| $f_p, friction$ | Friction force between piston and casing [N] |
| $f_c, friction$ | Friction force between casing and surroundings [N] |
| P | Pressure in gas spring chamber [Bar] |
| V | Volume of gas spring chamber [$m^3$] |
| $\alpha_e$ | Bandwidth of current controller [rad/s] |
| I | Integrator state variable |
| $R_a$ | Active damping [$\Omega$] |
| $\lambda$ | Leakage term in SCVM |
| $\alpha_0$ | Bandwidth of lowpass filter in SCVM [rad/s] |
| $\Psi$ | Rotor flux [Wb] |
| T | Sample time [s] |
| $U_{inj}$ | Injected voltage used in Square Wave Injection [V] |
| $U_h$ | Amplitude of injected voltage [V] |
| $\rho$ | Bandwidth of PLL [rad/s] |

**Table 4:** Resonator machine parameters

| Motor parameter | Notation | Value | Unit |
|---|---|---|---|
| Stator resistance | R | 4.725 | mΩ |
| Direct Stator Inductance | $L_d$ | 1 | mH |
| Quadrature Stator Inductance | $L_q$ | 0.66 | mH |
| Permanent magnet flux linkage | $\Psi_{PM}$ | 0.096 | Wb |
| Pole pairs | $n_p$ | 5 | |
| Pole pitch | $\tau$ | 15 | mm |
| Mass of casing | $m_c$ | 15 | kg |
| Mass of piston | $m_p$ | 5 | kg |
| Initial length of gas spring chambers | $x_g$ | 50 | mm |
| Cross-section area of gas spring chambers | A | $3.1 \cdot 10^{-3}$ | $m^2$ |
| Pressure in gas spring chambers | $p_0$ | 10 | Bar |
| External spring coefficient | $k_1$ | $10^5$ | N/m |
| Coulomb friction for piston | $C_{p,fr}$ | 10 | N |
| Coulomb friction for casing | $C_{c,fr}$ | 1 | N |
| Stribeck friction for piston | $S_{p,fr}$ | 50 | N |
| Stribeck friction for casing | $S_{c,fr}$ | 5 | N |
| Stribeck speed factor for piston | $k_p$ | 5 | s/m |
| Stribeck speed factor for casing | $k_c$ | 10 | s/m |
| Viscous friction for piston | $V_{p,fr}$ | 100 | Ns/m |
| Viscous friction for casing | $V_{c,fr}$ | 10 | Ns/m |
| Switching frequency | $f_s$ | 20 | kHz |
| DC link voltage | $U_{dc}$ | 180 | V |

# Contents

# 1

# Introduction

*This chapter gives an general introduction to the subject and presents the aim and outline of the thesis.*

## 1.1 General

The Intergovernmental Panel on Climate Change(IPCC) has concluded that the consumption of fossil fuels is a significant factor to the increasing average temperature around the globe. The environmental changes due to the increasing temperature might result in catastrophic consequences [1]. Still the energy consumption around the world is increasing, consequently alternative sources of energy is needed [2].

Geo-thermal energy is one of many low emission energy sources. For geo-thermal energy sources to be feasible and profitable, drilling costs need to be reduced. The drilling costs are often representing 60-70% of the total project costs [3]. Percussive drilling is a technique that use repeated hammer strokes to crush the rock. It has been found interesting since it has been proven to be 300 to 1000 % more time effective compared to conventional rotational drilling technique when drilling at great depths and in very hard rock which is most often the case for geo-thermal drilling projects [4].

Percussive drilling can be used with several different driving techniques, for example pneumatic pressure, steam pressure, water pressure and electromechanical force [5]. Resonator AS in Norway is trying to take advantage of the benefits of a linear electric motor in a percussive drilling application. Therefore they are developing a Tubular Linear Permanent Magnet Synchronous Machine (TLPMSM) to be oscillated in resonance. A TLPMSM has a very good power to volume ratio due to good utilization of the stator windings and good efficiency due to its linear motion which makes it to a good candidate for the application [6].

The first description of this type of system was made in [7] where the idea of using gas springs together with a TLPMSM to achieve high power oscillation was presented. Previous linear electric machines in oscillatory operation was limited to 2 kW because of the mechanical springs were too weak. Using gas springs instead made higher power levels possible [7].

A first prototype developed at Resonator AS is described in [8] where the concept is tested further. The prototype is driven by a single phase permanent magnet machine and include an extra coil for measurement of the induced voltage by the moving magnets. The signal from the measurement coil was used as the control signal for the force producing main coil in a positive feedback loop. After the oscillations where kick started, the positive feedback loop made the prototype oscillate with its resonance frequency [8]. In [9] simulations were performed which suggested that resonance could be maintained during repeating impacts into a rock surface.

A second prototype was developed in 2011 and the design process is described in [10]. The new prototype had increased input power, power density and hammering frequency [10]. An open loop control strategy was proposed in [11] that considered the nonlinear characteristic of the gas springs. The idea of the strategy is that if all system parameters are well known, including the rock properties, an alternating voltage can drive the prototype at the resonance frequency. Would more power be needed during operation the voltage is increased, the frequency of the applied voltage must then also be increased correspondingly to still drive the system at the resonance frequency [11].

The next step in the evolution of the concept is to drive the resonator with a three phase TLPMSM. Three phases would utilize the windings better and increase the force density further [10]. The stroke length can also be increased which gives more time for the hammer to gain speed. This gives higher kinetic energy to the hammer bit and therefore also higher impact energy to the rock.

## 1.2 Aim

The aim is to propose a control strategy for a three phase TLPMSM in a percussive drilling application. The control strategy aims to oscillate the mechanical system at the resonance frequency.

## 1.3 Scope

The thesis will focus as much as possible on the electric power aspect of the problem. The mechanical system properties will be simplified and not covered in depth. Also the model describing the rock will be simplified. This is however not critical for the strategy used in this work since it does not depend on analytical models for the mechanical system or the rock. Testing of proposed control strategy will be done in simulations performed in MATLAB/Simulink.

## 1.4 Outline of this thesis

Chapter 2 gives a brief introduction to the subject. Percussive drilling, TLPMSMs and resonance are described before the construction and the intended operation characteristic of the resonator are presented.

Chapter 3 presents all the modelling used in the work. This include the electric and mechanical parts of the resonator, a simplified rock model and a three phase converter.

In Chapter 4 the current controller is presented.

Chapter 5 presents two different strategies to make the control system sensorless.

Chapter 6 presents the control strategy used to oscillate the mechanical parts of the resonator.

Chapter 7 contains a conclusion and some future work are proposed.

# 2

# Background and Theory

*This chapter presents background information for the thesis aiming to introduce the reader to the subject and to clarify issues. It also presents intended operation characteristic for the system.*

## 2.1 Percussive drilling and the Resonator

Percussive drilling is an old drilling technique which repeatedly uses kinetic energy from a hammer as impact energy to crush rocks. This technique was first used in an oil drilling application in the middle of the nineteenth century and started to interest researchers about hundred years later. The method caused interest since it was a more efficient way to make holes in hard brittle rocks compared to conventional rotating drilling [5]. One of the most important parameters of performance in drilling is Rate of Penetration (ROP) which is a measure of the drilling speed. When it comes to drilling in medium-hard granite, it has been showed that percussive drilling has a 2.3 times higher ROP than conventional rotating drilling methods [12].

There exist two different types of percussive drilling, namely Down the Hole drilling (DTH) and top hammer drilling. The difference is if the hammer is located in the bottom or at the top of the borehole. Since top hammer drilling has depth limitations it is less applicable for hydrocarbon or geothermal well drilling [13] and therefore only DTH drilling is covered in this work.

The concept is used with many different driving techniques for the drill, most common is to use either a pneumatic, hydraulic or water driven system [13]. However, those techniques have different disadvantages such as low efficiency and pressure fluctuations [5]. For that reason Resonator AS in Norway is developing a drill driven by a Tubular Linear Permanent Magnet Synchronous Machine (TLPMSM). The electric motor is easy to control and has good efficiency which are desirable properties for the application. This drilling system is referred to as the Resonator in this work, since it should be oscillated at its resonance frequency.

The Resonator consists of a piston with permanent magnets and a casing with stator windings, as can be seen in Figure 2.1. Between the piston and the casing there are two gas springs which have nonlinear force-displacement characteristics and two small mechanical springs which should make sure that the piston is located in the middle of the casing when the machine is at rest. The casing is also attached to the surroundings by an external spring. Furthermore the Resonator is tubular-symmetric and the casing seals the whole unit. The construction can be considered as a system that consists of two mass-damper-spring subsystems where the inner mass is the piston and the outer mass is the casing. It could also be seen in Figure 2.1 that the outer mass, the casing, is used to hammer into the rock.

## 2.2 Tubular linear permanent magnet synchronous motor

A TLPMSM produces, in distinction to a regular rotating motor, a linear, short-stroke motion. Despite this, the working principles are the same as for a rotating PMSM but since the motion is linear instead of rotating, the stator and rotor are configured in a slightly different way. The tubular shape utilizes the stator windings in a better way than a conventional rotating machine does. This is since the tubular shape does not require any non-force producing end-windings which are inevitable for a rotating machine. This makes the tubular linear permanent magnet machine very powerful with a high force to volume ratio [6].

In many applications it can be beneficial to use a motor which produce a linear motion without any need of gears or other mechanical linkages which will decrease the overall efficiency. In this work a TLPMSM is used as a linear hammer which has the advantage to be able to transmit power from a electric source to impact energy into rocks without gears, bearings and driving shaft [5].

The construction of the rotor and stator of the TLPMSM used in the Resonator is seen in Figure 2.2 where half of a cross section is visualized. It can be seen that the rotor is longer than the stator and that the machine has 12 slots and 14 poles where 10 of the poles is overlapped by the stator and in that sense are ”active” at a time. The pole pitch is 15 mm. The 12 slots are divided into four slots per phase where two coils are connected in parallel with the other two coils. The arrows on the rotor represent the polarity of the permanent magnets. It can be seen that the assemblage of the magnets will generate a saliency in the sense of

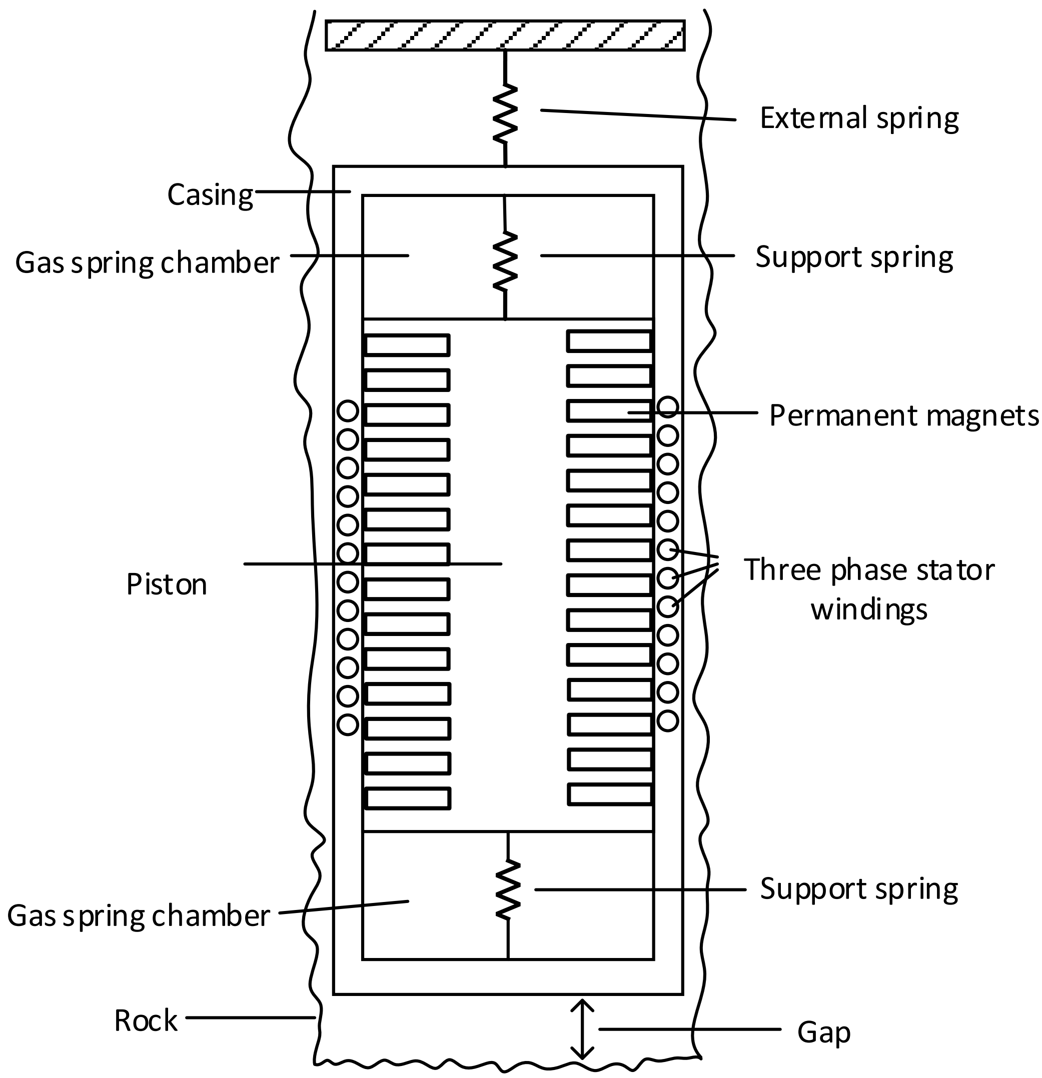


**Figure 2.1:** The most important parts of the Resonator.

different inductance depending on relative position. The magnetic flux is leaving the rotor through the iron represented by the yellow parts of the rotor in Figure 2.2 and returns through the red parts. This means that seen from the stator the inductance is highest when the magnetic flux is highest, which corresponds to higher inductance in the d-direction than in the q-direction. The three phase voltages applied to the stator are denoted as $u_a$, $u_b$ and $u_c$.

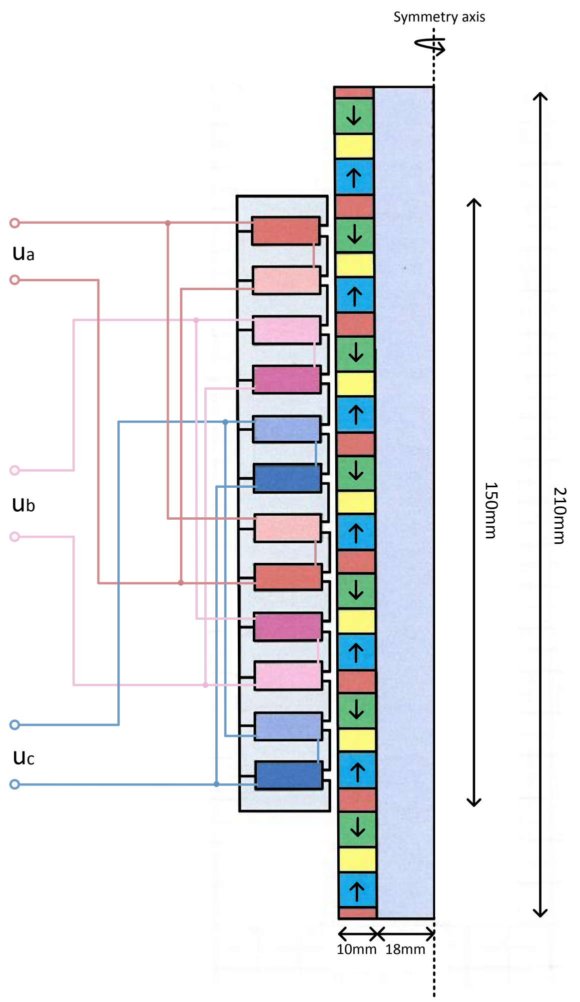


**Figure 2.2:** Rotor and stator of the TLPMSM. The arrows on the rotor represent permanent magnet polarity and $u_a$, $u_b$ and $u_c$.

## 2.3 Oscillation of undamped two degree of freedom system

Resonance is a vital part for the control strategy and the performance of the system. Resonance is a well known physical phenomenon which appears in many different areas of physical systems. Physical systems have a tendency to oscillate with larger amplitude for certain frequencies, those frequencies are called resonance frequencies or natural frequencies [14]. Also when an oscillating system is subjected to an external driving force, the amplitude is largest when the driving force has the same frequency as the natural frequency of the system [15].

When an ideal system oscillates at its resonance frequency it will oscillate with unchanged amplitude forever. The amplitude of the oscillations in a real world system will usually decrease due to losses, but the amplitude can be maintained if power supplied from an external source covers the losses.

In Section 2.1 it is seen that the drill consists of three springs and two masses where one of the masses is the stator and the other is the rotor of the TLPMSM. The stator is attached to the surroundings by a spring and the rotor is attached to the stator by two gas springs. This system is in this section simplified to an undamped two degree of freedom system consisting of two masses and two springs, visualized in Figure 2.3. In this simplified system, the mass to the left in Figure 2.3 corresponds to the stator and the other mass to the rotor. To simplify the calculations even further the the two masses and the two spring coefficients are considered equal.

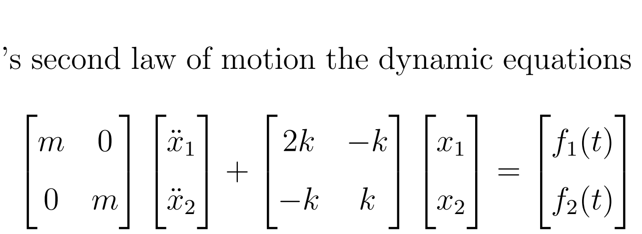


**Figure 2.3:** An undamped two degree of freedom system

From Newton's second law of motion the dynamic equations of the system can be written as

$$\begin{bmatrix} m & 0 \\ 0 & m \end{bmatrix} \begin{bmatrix} \ddot{x}_1 \\ \ddot{x}_2 \end{bmatrix} + \begin{bmatrix} 2k & -k \\ -k & k \end{bmatrix} \begin{bmatrix} x_1 \\ x_2 \end{bmatrix} = \begin{bmatrix} f_1(t) \\ f_2(t) \end{bmatrix} \tag{2.1}$$

where $f_1$ and $f_2$ are external forces acting on each mass and $x_1$ and $x_2$ are the positions of the masses relative the equilibrium position. The solution to (2.1) consists of two parts, a complementary and a particulary solution. The dynamic properties are coverd by the complementary solution which is obtained by setting the right side of (2.1) equal to zero. Since only the free oscillations are of interest here, only the complementary solution will be studied. Therefore, (2.1) reduce to

$$\begin{bmatrix} m & 0 \\ 0 & m \end{bmatrix} \begin{bmatrix} \ddot{x}_1 \\ \ddot{x}_2 \end{bmatrix} + \begin{bmatrix} 2k & -k \\ -k & k \end{bmatrix} \begin{bmatrix} x_1 \\ x_2 \end{bmatrix} = \begin{bmatrix} 0 \\ 0 \end{bmatrix}. \tag{2.2}$$

It is assumed that the system have harmonic motion in the following form

$$x_1(t) = X_1 cos(\omega_i t - \alpha) \tag{2.3a}$$
$$x_2(t) = X_2 cos(\omega_i t - \alpha) \tag{2.3b}$$

where $\omega_i$ is the natural frequency number $i$ for the system. The assumption in (2.3) means that if the system oscillates in any of its natural frequencies, $x_1$ and $x_2$ will have the same time dependence. It is also worth mentioning that free oscillations can only occur at the natural frequencies [16].

Equation (2.3) is substituted into (2.2) which results in

$$\begin{bmatrix} 2k - m\omega_i^2 & -k \\ -k & k - m\omega_i^2 \end{bmatrix} \begin{bmatrix} x_1 \\ x_2 \end{bmatrix} = \begin{bmatrix} 0 \\ 0 \end{bmatrix}. \tag{2.4}$$

Of course, only nontrivial solutions are of interest which is obtained by solving the characteristic equation of (2.4). This will result in

$$\omega_i^2 = \frac{3k}{2m} \pm \frac{\sqrt{5}k}{2m}. \tag{2.5}$$

Since $\omega_i \geq 0$ it exists two natural frequencies and it is not a coincident that this is the same as the number of degrees of freedom for the system [16]. From here on the natural frequencies will be denoted as $\omega_1$ and $\omega_2$ where $\omega_1 < \omega_2$. If those frequencies are substituted into the first equation of (2.4) the following relationships are obtained

$$\beta_1 = \frac{X_2}{X_1} = 1 - \frac{(3-\sqrt{5})^2 k}{m} \approx 1 - 0.29\frac{k}{m} \tag{2.6a}$$
$$\beta_2 = \frac{X_2}{X_1} = 1 - \frac{(3+\sqrt{5})^2 k}{m} \approx 1 - 13.7\frac{k}{m} \tag{2.6b}$$

where $\beta_1$ is obtained by substituting $\omega_1$ and $\beta_2$ is obtained by substituting $\omega_2$. If $\beta_1$ or $\beta_2$ have a negative value it means that the two masses are moving in different directions, they oscillate completely out of phase. This must be the case since the sign of the quotient of the speeds must be the same as the sign of the quotient of the positions when the masses have the same time dependence. If $\beta_1$ or $\beta_2$ have a positive value it is the opposite, they oscillate in phase. Since $k$ and $m$ always are greater than zero, it can be concluded from (2.6) that it is more likely for the two masses to oscillate in phase if the system oscillate with the same frequency as the lower of its two natural frequencies and out of phase if it oscillate at the higher of the frequencies. The first case is commonly referred to as a symmetric mode and the second case as an antisymmetric mode. It could be worth mentioning that a symmetric two degree of freedom system (which could have been the case if both masses had two attached springs) always have one symmetric and one antisymmetric mode independently of the ratio between spring coefficients and masses [16]. Furthermore, the frequency of the symmetric mode is always lower than for the antisymmetric mode [16].

## 2.4 Operation characteristic of the Resonator

The electric force should be used to bring the system in resonance. When the system is in resonance only a small amount of electric energy is needed to maintain the oscillation. The oscillating behavior should be used for percussive drilling with very low energy consumption.

The resonance frequencies for the two mass-damper-spring systems could be determined by solving the differential equations for the system as was indicated in Section 2.3. Since the system has two degrees of freedom it will have two resonance frequencies. When the system works at the lowest of the two frequencies, the piston and the casing oscillate in phase. It means that it is a maximum for the stroke length for both the piston and the casing, but not for the relative motion between the piston and the casing. When the system is working at the larger of the two frequencies, the piston and the casing oscillate completely out of phase. It means that also the relative motion between the piston and the casing has a maximum.

The best working point for the system is at the higher of the two frequencies. When the relative motion between the piston (rotor) and the casing (stator) has a maximum, also the back-EMF has a maximum which means that the current, for a fixed voltage, has a minimum. This will result in low copper losses.

# 3

# Modeling

*The aim of this chapter is to present the models used in the rest of the work. The chapter will first introduce three phase systems and Clark and Park transformations. Then a dynamic model of an TLPMSM is presented followed by a description of a Simulink implementation of a converter with a carrier wave comparison switching technique. Moreover, models of the mechanical parts of the resonator are presented followed by a model of a hard rock.*

## 3.1 Three phase systems

The stator windings of three phase machines are usually connected to three phases whose voltages are phase shifted $120^o$. The three phases are denoted a, b and c and the voltages can be expressed as

$$u_a(t) = U_a cos(\omega_r t + \varphi_a) \tag{3.1a}$$
$$u_b(t) = U_b cos(\omega_r t - 120^o + \varphi_b) \tag{3.1b}$$
$$u_c(t) = U_c cos(\omega_r t - 240^o + \varphi_c), \tag{3.1c}$$

where $U_a$, $U_b$ and $U_c$ are the amplitudes of the phase voltages and $\varphi_a$, $\varphi_b$ and $\varphi_c$ are angle offsets for the phase voltages. A three phase system is usually designed to be as symmetric as possible which means that for an ideal case should $U_a = U_b = U_c = U$ and $\varphi_a = \varphi_b = \varphi_c = \varphi$ [17]. If this is fulfilled the main advantages with three phase systems are obtained which are

- The sum of the instantaneous phase powers is constant.
- The sum of the phase voltages is always zero [17].

### 3.1.1 Clarke and Park transformation

Since the sum of the phase voltages for a symmetric three phase system is zero, one voltage can always be expressed as a sum of the other two

$$u_a(t) + u_b(t) + u_c(t) = 0 \Rightarrow u_c(t) = -(u_a(t) + u_b(t)). \tag{3.2}$$

Since one voltage is always determined by the other two it is unnecessary to express all three voltages. The three phase voltages could, without loss of information, be expressed in an equivalent two phase system. The Clarke transformation uses two perpendicular axes, $\alpha$ and $\beta$, which could be considered as the real and imaginary axis of a complex plane. The transformation from the three phase system to the complex plane is calculated as

$$\begin{bmatrix} u_\alpha(t) \\ u_\beta(t) \end{bmatrix} = K \begin{bmatrix} \frac{2}{3} & -\frac{1}{3} & -\frac{1}{3} \\ 0 & \frac{1}{\sqrt{3}} & \frac{1}{\sqrt{3}} \end{bmatrix} \begin{bmatrix} u_a(t) \\ u_b(t) \\ u_c(t) \end{bmatrix}, \tag{3.3}$$

where $K$ is a scaling constant which can be arbitrarily chosen, but some values are more practical than others. In this work $K = 1$ is used which is referred to as peak-value scaling [17]. The complex voltage vector is a rotating vector in the complex plane and could also be expressed as

$$\mathbf{u}^s(t) = KUe^{j(\omega_r t + \gamma)} \tag{3.4}$$

where it is seen that the vector rotates with the same frequency as the phase voltages. For control purposes it is more useful to transform (3.4) to a complex plane rotating synchronously with the vector itself. This could be done with the Park transformation,

$$\mathbf{u}^r(t) = \mathbf{u}^s(t)e^{-j\theta} = KUe^{j\gamma} = u_d + ju_q, \tag{3.5}$$

where $\theta$ is the electrical angle in which the rotor flux is directed. The angle could be selected arbitrarily but this is a common choice when it comes to electric machine control [17]. The selection makes it possible to decouple the torque and flux producing currents. The axis aligned with the flux is commonly referred to as the d-axis and the axis perpendicular to the flux as the q-axis, which is why this transformation often is called dq-transformation [17].

## 3.2 Dynamic model of the TLPMSM

The aim of this section is to derive a dynamic model of the electric part of the TLPMSM. Since the model should be used for control purpose it is performed in dq-coordinates. The following assumptions are made:

- The flux density in the air gap is sinusoidally distributed.
- No cogging force.
- No magnetic saturation.
- No iron losses.
- The resistance is independent of frequency and temperature.

The voltage applied to the stator gives a voltage over the stator resistance and an induced voltage according to

$$u_d = Ri_d + \frac{d\Psi_d}{dt} - \omega_r \Psi_q \tag{3.6a}$$
$$u_q = Ri_q + \frac{d\Psi_q}{dt} + \omega_r \Psi_d, \tag{3.6b}$$

where $u_d$ and $u_q$ are the stator voltage in d- respectively q-direction, $R$ is the resistance in the stator windings, $\Psi_d$ and $\Psi_d$ are the stator flux linkage in d- and q-direction respectively and the last term in the expressions come from the transformation from $\alpha\beta$- to dq-coordinates. The rotor flux is aligned with the d-axis which means that the flux linkage can be written as

$$\Psi_d = L_d i_d + \Psi_{PM} \tag{3.7a}$$
$$\Psi_q = L_q i_q, \tag{3.7b}$$

where $L_d$ and $L_q$ are the inductances in d- and q-direction respectively and $\Psi_{PM}$ is the flux from the permanent magnets. By inserting (3.7) in (3.6) the following expressions are obtained,

$$u_d = Ri_d + L_d \frac{di_d}{dt} - \omega L_q i_q \tag{3.8a}$$
$$u_q = Ri_q + L_q \frac{di_q}{dt} + \omega L_d i_d + \omega \Psi_{PM}. \tag{3.8b}$$

where $\omega L_q i_q$ and $\omega L_d i_d$ will be denoted as cross coupling terms and $\omega \Psi_{PM}$ as the back electromotive force (back-emf). Since both the rotor and the stator are allowed to move it is the relative position and motion between them which is important [5]. The angular speed of the flux from the permanent magnets can be expressed as

$$\omega = \frac{\pi(v_p - v_c)}{\tau}, \tag{3.9}$$

where $v_p$ is the velocity of the piston, $v_c$ is the velocity of the casing and $\tau$ is the pole pitch. In (3.9) it can be seen that angular speed and linear speed are related by $\pi$ divided by the pole pitch. The same relationship holds for electrical angle and linear position.

The force is generated by the interaction of the flux generated by the current in the stator windings and the flux generated by the permanent magnets integrated in the piston. The two flux vectors attracts each other and a force is produced forcing them to align. The larger the electrical angle is between the vectors the higher the force is, up to a maximum at 90°. The force produced by the machine is calculated as

$$F_e = \frac{3n_p\pi}{2\tau}(\Psi_d i_q - \Psi_q i_d) = \frac{3n_p\pi}{2\tau}[\Psi_{PM} + (L_d - L_q)i_d]i_q \tag{3.10}$$

where $n_p$ is the number of pole pairs and $\tau$ is the pole pitch [5]. The current reference in d-direction usually is set to zero which means that the force could be controlled by controlling the current in q-direction [5]. As can be seen in (3.10), $i_d$ can also be used to produce force. But since the value of the saliency is small compared to the value of the flux it is better to set the d-current reference to zero.

## 3.3 Pulse Width Modulation and three phase converter

To make the simulations in later chapters more realistic, a three phase converter, seen in Figure 3.1, is also included in the simulations. The converter can be modelled in more detail than is done here where the switches are assumed to be ideal. The model will therefore not include switching losses, conduction losses or blanking time since the focus in this work is on the Resonator rather than on the converter. However, the current ripple in the stator windings generated by the switching will be captured in the simulations.

There are several ways of performing the switching for a three phase converter, in this work pulse width modulation (PWM) is used where a carrier wave is compared to a reference value to determine the moments for switching. As is shown in Figure 3.2, when the reference is lower than the carrier wave, $-U_{dc}/2$ is applied and when the reference is higher then the carrier wave $U_{dc}/2$ is applied. The peak voltage with this technique can maximally be half of the DC-link voltage [18].

The converter and the carrier wave comparison technique are implemented in Simulink in two steps. The first step is the switching which is implemented by using

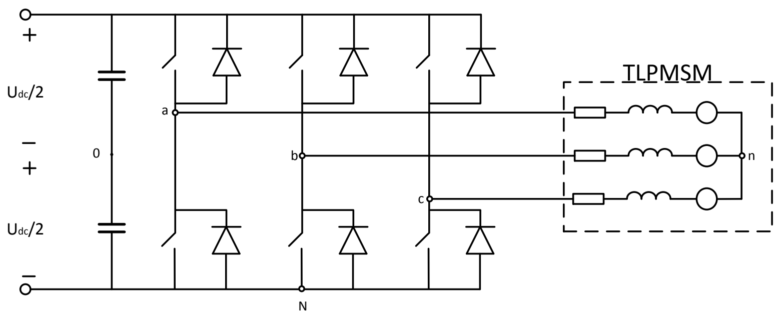


**Figure 3.1:** Three phase converter.

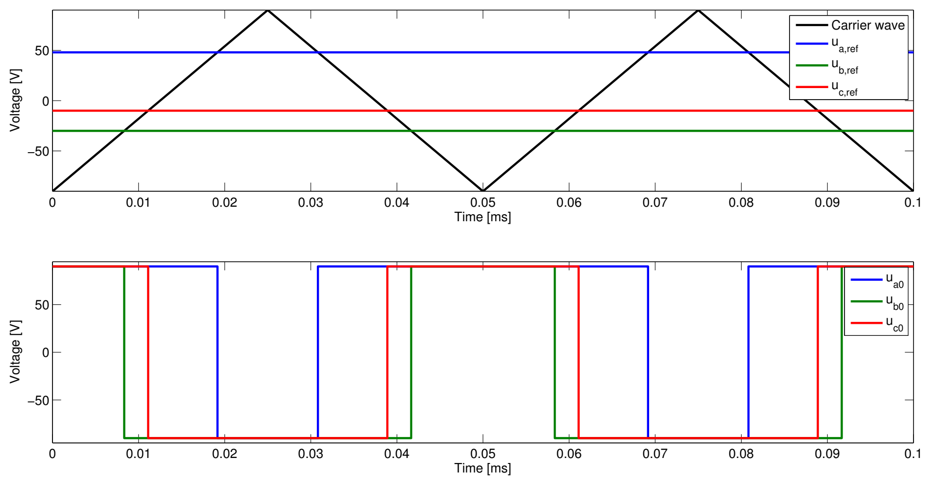


**Figure 3.2:** PWM switching pattern for the three phases.

comparators as can be seen in Figure 3.3b. This gives a pulse shaped voltage to the machine. The second step is to recalculate the converter voltage to the phase voltage of the machine since the dynamics of the machine are expressed in phase voltages. The converter voltage can be expressed in terms of machine phase voltage as

$$\begin{bmatrix} u_{a0} \\ u_{b0} \\ u_{c0} \end{bmatrix} = \begin{bmatrix} u_{an} + u_{n0} \\ u_{bn} + u_{n0} \\ u_{cn} + u_{n0} \end{bmatrix}. \tag{3.11}$$

Since the phase voltages of the machine sum up to zero, the following equation is obtained by adding the three equations in (3.11) together,

$$3u_{n0} = u_{a0} + u_{b0} + u_{c0}. \tag{3.12}$$

By combining (3.11) and (3.12) it is straight forward to obtain the expressions for the phase voltages of the machine based on the output voltage of the converter, as

$$\begin{bmatrix} u_{an} \\ u_{bn} \\ u_{cn} \end{bmatrix} = \begin{bmatrix} u_{a0} - u_{n0} \\ u_{b0} - u_{n0} \\ u_{c0} - u_{n0} \end{bmatrix} = \begin{bmatrix} \frac{2u_{a0} - u_{b0} - u_{c0}}{3} \\ \frac{2u_{b0} - u_{a0} - u_{c0}}{3} \\ \frac{2u_{c0} - u_{a0} - u_{b0}}{3} \end{bmatrix}. \tag{3.13}$$

Equation (3.13) is implemented in Simulink as seen in Figure 3.3c.

## 3.4 Mechanical modeling

This section aims to present analytical expressions for the mechanical system of the resonator. The main parts of the mechanical system are the piston, the casing and the two gas springs between the piston and casing.

### 3.4.1 Gas spring

The most important motivation for using gas springs in this application is that they will not wear down as springs made of steel will do. The gas springs used in this application can be made very stiff which allows a relatively fast oscillation for the heavy piston [7]. In theory the force from a gas spring can be infinite but in reality the limiting factor is the durability of the chamber enclosing the gas. An ideal gas enclosed in a chamber undergoing a reversible adiabatic process follows the relation

$$PV^{\alpha} = constant \tag{3.14}$$

where $P$ is pressure of the gas, $V$ is volume of the gas and $\alpha$ is the adiabatic constant of the gas [19]. From Figure 3.4 it can be seen that the volume of the upper chamber, $V_u$, and the volume of the lower chamber, $V_l$, can be expressed as

$$V_u = A(x_g + x) \tag{3.15a}$$
$$V_l = A(x_g - x) \tag{3.15b}$$

where $A$ is the cross-section area of the chambers, $x_g$ is the initial length of the chambers and $x = x_p - x_c$. A force from the gas springs act on the piston if a

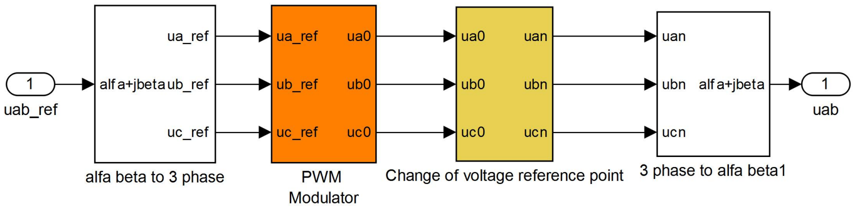


**(a)** Converter and PWM.

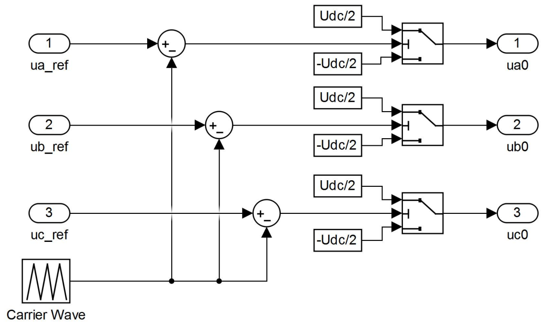


**(b)** The blocks inside the subsystem "PWM Modulator".

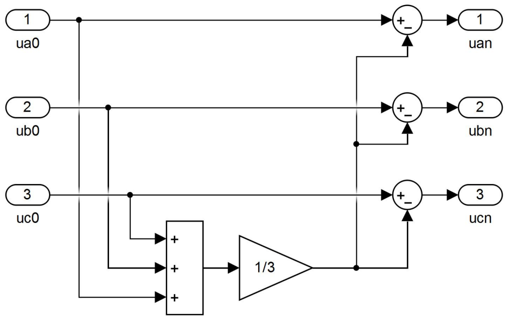


**(c)** The blocks inside the subsystem "Change of voltage reference point".

**Figure 3.3:** Converter and PWM implementation in Simulink.

pressure difference occur between upper and lower chamber. This force is expressed as

$$f_{gas} = A(P_u - P_l) = Ap_0\Big(\Big(\frac{x_g}{x_g + x}\Big)^{\alpha} - \Big(\frac{x_g}{x_g - x}\Big)^{\alpha}\Big) \tag{3.16}$$

where $p_0$ is the initial pressure in the chambers. Since the initial pressure are assumed to be the same in both chambers, $f_{gas}$ is acting to put the piston in a position where x=0. It can also be seen that the initial pressure can be adjusted to alter the stiffness of the springs.

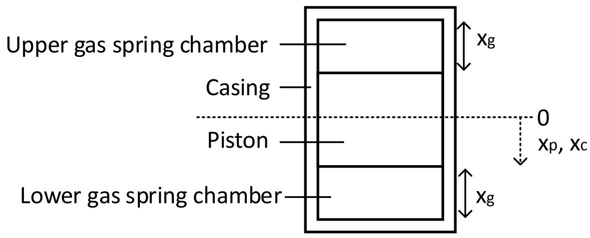


**Figure 3.4:** Gas springs between piston and casing.

### 3.4.2 Piston

The piston is the rotor for the TLPMSM. As can be seen in Figure 3.5, a electromagnetic force, friction and a force from the gas spring are acting on the piston. Since both the piston and the casing are moving, the forces from the friction and the gas springs depend on the relative motion and displacement between the piston and casing.

As low and zero speed is a part of the system's working region the friction is modelled as a combination of viscous damping, Coulomb damping and Stribeck damping [20]. An expression for the friction force can be expressed as

$$f_{p,friction} = C_{p,fr}sign(\dot{x_p} - \dot{x_c}) + V_{p,fr}(\dot{x_p} - \dot{x_c}) + S_{p,fr}e^{-k_p|\dot{x_p} - \dot{x_c}|}sign(\dot{x_p} - \dot{x_c}), \tag{3.17}$$

where $C_{p,fr}$ is a Coulomb coefficient, $V_{p,fr}$ is a viscous coefficient, $S_{p,fr}$ is a Stribeck coefficient and $k_p$ is a Stribeck speed factor [20]. Equation (3.17) is visualized in Figure 3.6.

According to Newtons second law, the motion equation for the piston is expressed as

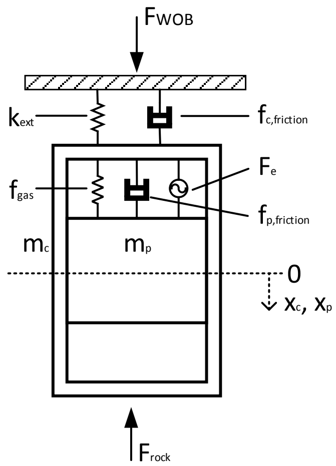


**Figure 3.5:** Mechanical model of the resonator.

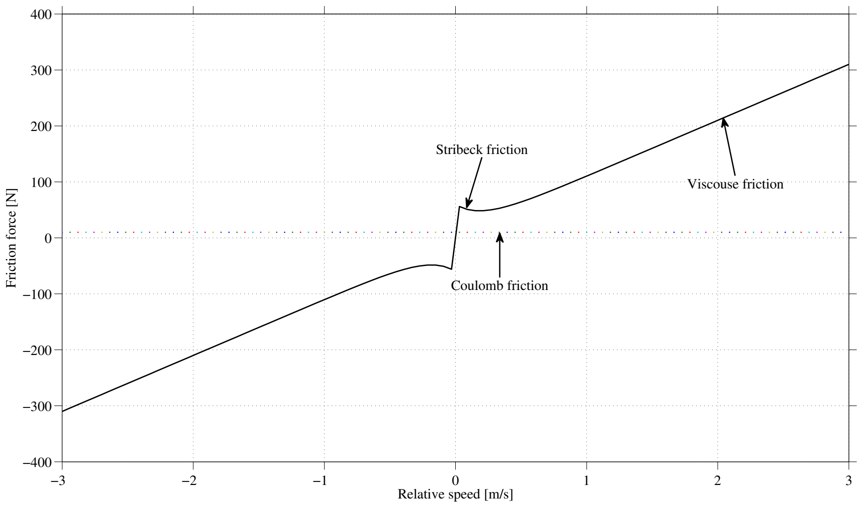


**Figure 3.6:** Friction force between piston and casing.

$$m_p \ddot{x_p} = F_e - f_{p,friction} - f_{gas} + m_p g = f_{piston} \tag{3.18}$$

where $F_e$ is the electromechanical force, $m_p g$ is the gravitational force and $f_{gas}$ is seen in (3.16).

### 3.4.3 Casing

According to Newton's third law, the casing is subjected to a counter-force from the piston. It is also, as seen in Figure 3.5, subjected to a friction force, a force from the external mechanical spring that follows Hooke's law and a force from the rock surface during an impact. A model of the force from the rock is presented in Section 3.5. The force $F_{WOB}$, in Figure 3.5, is used to press the Resonator towards the rock. The subscript "WOB" is an abbreviation of "Weight On Bit" since the force is generated by a weight located on top of the Resonator. Applying Newton's second law results in

$$m_c\ddot{x}_c = -f_{piston} - f_{c,friction} - k_{ext}x_c - f_{rock} + F_{WOB} + m_c g \tag{3.19}$$

where $k_{ext}$ is the spring coefficient of the external spring and $f_{rock}$ is described further in Section 3.5. The friction force, $f_{c,friction}$ is modeled in the same way as the piston friction,

$$f_{c,friction} = C_{c,fr}sign(\dot{x_c}) + V_{c,fr}(\dot{x_c}) + S_{c,fr}e^{-k_c|\dot{x_c}|}sign(\dot{x_c}). \tag{3.20}$$

## 3.5 Rock modeling

Percussive drilling is used for its good performance for drilling in hard rocks and therefore only a model of a hard rock is considered here. It does not exist a clear definition of what the strength of a rock is. Different rocks behave differently under varying conditions. But in general granite, limestone, sandstone, quartz among others are considered as hard [13].

Several approaches to modeling rocks can be found in the literature but in this project a simplified version of the model presented in [21][22] is used. It has been indicated that hard rocks deform linearly until a sudden failure [23] and that they before the failure have a visco-elastic behavior [21]. After the failure the rock is crushed and the rock cuttings are removed from the borehole. It is indicated in the literature that the ROP is challenging to predict since the behavior of the rock after the failure is very complex. This is why the rock model in this work is simplified to only the viscous damping and a linear compressive spring which means that the model do not include the crushing process. The linear spring represents the built up counter force in the rock during the impact and the viscous damping is representing the power absorbed by the rock. In Figure 3.7 the adopted rock model is seen along with the rest of the mechanical system presented in Section 3.4. The equation for the force from the rock acting on the casing is written as

$$f_{rock} = d(k_r(x_c - gap) + b_r\dot{x}_c) \tag{3.21}$$

where $d = \begin{cases} 1, & when\ x_c \geq gap \\ 0, & when\ x_c < gap \end{cases}$.

The rock is included in the models by rewritting (3.19) as,

$$m_c\ddot{x}_c = -f_{net} - f_{c,friction} - k_1 x_c - d(k_r(x_c - gap) + b_r\dot{x}_c). \tag{3.22}$$

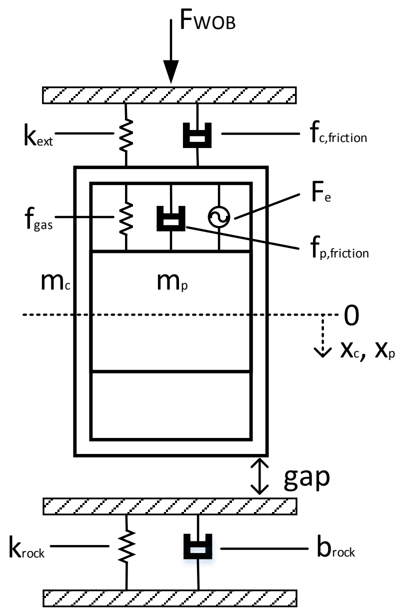


**Figure 3.7:** Complete mechanical system.

In the work a rock type called Hackensack Siltstone have been considered. It is a hard rock type with $k_{rock} = 2.23 \cdot 10^9$ N/m and $b_{rock} = 2.3 \cdot 10^5$ Ns/m [21].

# 4

# Current controller

*As was seen in Chapter 3, the force produced by the TLPMSM is proportional to the q-current when the d-current is set to zero. This means that the force could be controlled by transforming the force reference to a q-current reference with (3.10) and controlling the q-current. The presented current controller is based on a standard vector control scheme.*

## 4.1 Design of current controller

The electric part of the TLPMSM is described by (3.8) where it can be seen that the d- and q-systems are coupled with the cross-coupling terms. If the cross-coupling terms are compensated for, the electric system can be described as two SISO (single input single output) systems. Furthermore, it is possible to make a feed forward of the back-EMF which otherwise will act as a disturbance to the current controller. With exact compensations (3.8) reduce to

$$u_d = Ri_d + L_d \frac{di_d}{dt} \tag{4.1a}$$

$$u_q = Ri_q + L_q \frac{di_q}{dt}. \tag{4.1b}$$

With the compensations, the currents in d- and q-direction can be controlled independently of each other. Laplace transformation of (4.1) gives

$$G_d(s) = \frac{I_d(s)}{U_d(s)} = \frac{1}{sL_d + R} \tag{4.2a}$$

$$G_q(s) = \frac{I_q(s)}{U_q(s)} = \frac{1}{sL_q + R}. \tag{4.2b}$$

Two PI-controllers will be created for the currents, one for the d-direction and one for the q-direction. The design approach that will be used is loop shaping, which means that the controllers are selected to give the closed loop systems desired properties. In this work the controllers are selected to make the closed loop systems respond like two first order systems with a selectable bandwidth, $\alpha_e$,

$$G_{cd}(s) = \frac{F_d(s)G_d(s)}{1 + F_d(s)G_d(s)} = \frac{\alpha_e}{s + \alpha_e} \tag{4.3a}$$

$$G_{cq}(s) = \frac{F_q(s)G_q(s)}{1 + F_q(s)G_q(s)} = \frac{\alpha_e}{s + \alpha_e}. \tag{4.3b}$$

It can be concluded from (4.3) that the controllers should be selected as

$$F_d(s) = \frac{\alpha_e}{s} G_d^{-1}(s) = \alpha_e \hat{L}_d + \frac{\alpha_e \hat{R}}{s} \tag{4.4a}$$

$$F_q(s) = \frac{\alpha_e}{s} G_q^{-1}(s) = \alpha_e \hat{L}_q + \frac{\alpha_e \hat{R}}{s}. \tag{4.4b}$$

A drawback of this design approach is sensitivity to disturbances [17]. It is intuitive that robustness to disturbances can be improved by increasing the integral part of the controllers, but this will also reduce the phase margin which of course is undesirable. By looking at (4.3) and (4.4) it can be seen that the integral part of the controllers can be increased without any reduction in phase margin if the resistance in the windings is increased equally much. This is of course not a good idea because then the copper losses will be increased. A better approach is to add active damping. Active damping is a trick that adds a fictive resistance to the windings in the machine which increases the integral action without any reduction of the phase margin or additional losses [17]. With active damping (4.2) change to

$$G'_d(s) = \frac{1}{sL_d + R + R_{ad}} \tag{4.5a}$$

$$G'_q(s) = \frac{1}{sL_q + R + R_{aq}}. \tag{4.5b}$$

The active damping is recommended in [17] to be selected to give $G'_d(s)$ and $G'_q(s)$ the same bandwidth as the closed loop systems. This gives

$$\frac{\hat{R}+R_{ad}}{\hat{L}_d} = \alpha_e \Rightarrow R_{ad} = \alpha_e \hat{L}_d - \hat{R} \tag{4.6a}$$

$$\frac{\hat{R}+R_{aq}}{\hat{L}_q} = \alpha_e \Rightarrow R_{aq} = \alpha_e \hat{L}_q - \hat{R}. \tag{4.6b}$$

With active damping the controllers change to

$$F_d(s) = \frac{\alpha_e}{s} G_d^{-1}(s) = \alpha_e \hat{L}_d + \frac{\alpha_e(\hat{R}+R_{ad})}{s} \tag{4.7a}$$

$$F_q(s) = \frac{\alpha_e}{s} G_q^{-1}(s) = \alpha_e \hat{L}_q + \frac{\alpha_e(\hat{R}+R_{aq})}{s}. \tag{4.7b}$$

The controllers are very easy to tune since the only tuning parameter is the bandwidth, $\alpha_e$. When the current controllers are designed it is assumed that the voltage reference from the current controller is applied to the motor in an ideal manner. This assumption is only valid if the bandwidth is selected much lower than the bandwidth of the power electronic converter [17].

### 4.1.1 Integrator anti windup

In all real systems there exist certain limits to the control signals. In this work the voltage is limited by the DC-link voltage of the converter, which should supply the requested voltage. Due to this a situation can occur where the voltage can not reach the voltage reference calculated by the current controller. When this happens, the integrator in the controller integrates the error even if the current is uncontrolled. When the error finally is reduced to zero the integrated error stored in the integrator is too large to hold the error to zero. Instead, the integrator must integrate an error with opposite sign before the reference could be reached. This phenomenon is referred to as integrator windup [17].

To overcome integrator windup the error is "back calculated" when the voltage limit is reached. This well known method is described in [17]. If $\boldsymbol{u_{ideal}}$ is introduced as the ideal output voltage vector from the current controllers and $\pm U_{dc}/2$ are the limits of the frequency converter, a limited voltage can be introduced as

$$|\boldsymbol{u}| = s(\boldsymbol{u_{ideal}}) = \begin{cases} |\boldsymbol{u_{ideal}}|, & |\boldsymbol{u_{ideal}}| \le U_{dc}/2 \\ U_{dc}/2, & |\boldsymbol{u_{ideal}}| > U_{dc}/2, \end{cases} \tag{4.8}$$

where $\boldsymbol{u}$ is the voltage vector from the current controller. The PI controller could be described as

$$\boldsymbol{I} = \begin{bmatrix} I_d \\ I_q \end{bmatrix} = \begin{bmatrix} \int \epsilon_d dt \\ \int \epsilon_q dt \end{bmatrix} \tag{4.9a}$$

$$\boldsymbol{u_{ideal}} = \begin{bmatrix} u_{ideal,d} \\ u_{ideal,q} \end{bmatrix} = \begin{bmatrix} \alpha_e \hat{L}_d \epsilon_d + \alpha_e(\hat{R} + R_{ad}) I_d \\ \alpha_e \hat{L}_q \epsilon_q + \alpha_e(\hat{R} + R_{aq}) I_q \end{bmatrix} \tag{4.9b}$$

$$|\boldsymbol{u}| = s(\boldsymbol{u_{ideal}}) \tag{4.9c}$$

$$\boldsymbol{u} = |\boldsymbol{u}| e^{jarg(\boldsymbol{u_{ideal}})} \tag{4.9d}$$

where $\boldsymbol{I}$ is the state variable of the integrators. When the voltage limit is reached the errors are "back calculated" and are denoted as $\bar{\epsilon}_d$ and $\bar{\epsilon}_q$. Then (4.9b) could be expressed as

$$\boldsymbol{u} = \begin{bmatrix} u_d \\ u_q \end{bmatrix} = \begin{bmatrix} \alpha_e \hat{L}_d \bar{\epsilon}_d + \alpha_e(\hat{R} + R_{ad}) I_d \\ \alpha_e \hat{L}_q \bar{\epsilon}_q + \alpha_e(\hat{R} + R_{aq}) I_q \end{bmatrix} \tag{4.10}$$

By subtracting (4.9b) of (4.10) and solving for $\bar{\boldsymbol{\epsilon}}$ the following is obtained

$$\bar{\boldsymbol{\epsilon}} = \begin{bmatrix} \bar{\epsilon}_d \\ \bar{\epsilon}_q \end{bmatrix} = \begin{bmatrix} \epsilon_d + \frac{1}{\alpha_e \hat{L}_d}(u_d - u_{ideal,d}) \\ \epsilon_q + \frac{1}{\alpha_e \hat{L}_q}(u_q - u_{ideal,q}) \end{bmatrix} \tag{4.11}$$

This error is used for (4.9a) which implies that (4.9) is changed to

$$\boldsymbol{I} = \begin{bmatrix} I_d \\ I_q \end{bmatrix} = \begin{bmatrix} \int \epsilon_d + \frac{1}{\alpha_e \hat{L}_d}(u_d - u_{ideal,d}) dt \\ \int \epsilon_q + \frac{1}{\alpha_e \hat{L}_q}(u_q - u_{ideal,q}) dt \end{bmatrix} \tag{4.12a}$$

$$\boldsymbol{u_{ideal}} = \begin{bmatrix} u_{ideal,d} \\ u_{ideal,q} \end{bmatrix} = \begin{bmatrix} \alpha_e \hat{L}_d \epsilon_d + \alpha_e(\hat{R} + R_{ad}) I_d \\ \alpha_e \hat{L}_q \epsilon_q + \alpha_e(\hat{R} + R_{aq}) I_q \end{bmatrix} \tag{4.12b}$$

$$|\boldsymbol{u}| = s(\boldsymbol{u_{ideal}}) \tag{4.12c}$$

$$\boldsymbol{u} = |\boldsymbol{u}| e^{j \cdot arg(\boldsymbol{u_{ideal}})} \tag{4.12d}$$

Note that (4.12) is exacly the same as (4.9) if the voltage limit is not reached. When the controllers are implemented in a microprocessor, all calculations and measurements are performed in discrete time which means that also the control algorithm must be in discrete time. Here forward Euler is used which means that a derivative is approximeted as

$$\frac{dx(t)}{dt} \approx \frac{x(t+T)-x(t)}{T}, \tag{4.13}$$

where T is the sampling period. With this method a discrete version of (4.12) is obtained as

$$\boldsymbol{I_{k+1}} = \begin{bmatrix} I_{d,k} + T\Big(\epsilon_{d,k} + \frac{1}{\alpha_e \hat{L}_d (u_{ideal,d,k} - u_{d,k})}\Big) \\ I_{q,k} + T\Big(\epsilon_{q,k} + \frac{1}{\alpha_e \hat{L}_q (u_{ideal,q,k} - u_{q,k})}\Big) \end{bmatrix} \tag{4.14a}$$

$$\boldsymbol{u_{ideal,k}} = \begin{bmatrix} \alpha_e \hat{L}_d \epsilon_{d,k} + \alpha_e(\hat{R} + R_{ad}) I_{d,k} \\ \alpha_e \hat{L}_q \epsilon_{q,k} + \alpha_e(\hat{R} + R_{aq}) I_{q,k} \end{bmatrix} \tag{4.14b}$$

$$|\boldsymbol{u_k}| = s(\boldsymbol{u_{ideal,k}}) \tag{4.14c}$$

$$\boldsymbol{u_k} = |\boldsymbol{u_k}| e^{j \cdot arg(\boldsymbol{u_{ideal,k}})}, \tag{4.14d}$$

where the sampling period is $T = 1/f_s = 50\ \mu s$.

## 4.2 Evaluation of Current controller

In this section the current controller is investigated in terms of pole and zero placement and with simulations both for an ideal case when the parameters are perfectly estimated and when they are afflicted with errors. All of the analysis is done for the q-current but the same analysis could just as well be done for the d-current.

### Evaluation of current controller with perfect parameters

A current controller with perfect parameters means that the estimated parameters used in the controller have exactly the same values as the real parameters in the machine. The current controller is evaluated in this ideal case to ensure that its behavior corresponds to the design. In Figure 4.1a two step responses are visualized, one with the continuous controller described in (4.12) and one with the discrete controller described in (4.14). It can be seen that the step response with the continuous controller is shaped as a first order system with a rise time corresponding to the selected bandwidth,

$$t_r = \frac{ln9}{\alpha_e} = \frac{ln9}{5000} \approx 0.44\, ms. \tag{4.15}$$

This is interpreted as that the loop shaping design for the continuous current controller is working. For the discrete controller it can be seen that it is faster than the continuous case for the first few samples, before it gets slower. This can be explained by the sampling. In the beginning when the error is continuously reducing for the continuous controller, the error for the discrete controller is reduced in steps. This increases the proportional action for the discrete controller which makes it faster in the beginning. After about 0.1 ms, in Figure 4.1a, the output from the controllers are dominated by the integrators. The integrator reacts to the sampling opposite to the proportional part. Since it is updated in steps, the integrator action is reduced by the sampling which, after a while, makes the step response slower.

To make the current step response with the discrete controller more similar to the case with the continuous controller, the integral action for the discrete controller can be increased. In Figure 4.1b the integral action for the discrete controller is increased by 1.45 times which makes the step response much more similar to the step response with the continuous controller in Figure 4.1a.

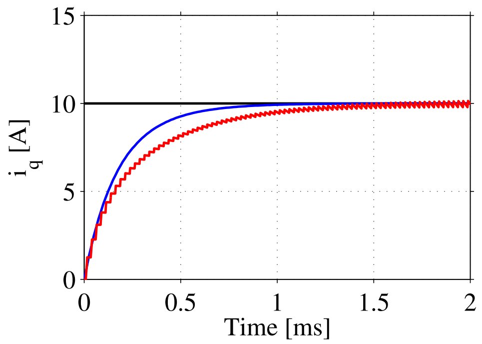


**(a)** Step response in the current with $\alpha_e =$ 5000 rad/s and with the same integral action for both controllers. The blue line is simulated with the continuous controller and the red line with the discrete controller.

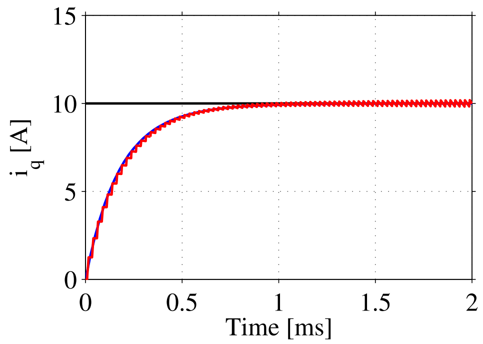


**(b)** Step response in the current with $\alpha_e =$ 5000 rad/s and with increased integral action with 1.45 times for the discrete controller. The blue line is simulated with the continuous controller and the red line with the discrete controller.

**Figure 4.1:** Current step response with continuous and discrete current controllers.

To improve the robustness to disturbances, active damping was added. Active damping should not change the dynamics of the system, only improve its robustness. This can be seen by looking at the closed loop system from current reference to actual current. In the q-direction with perfect parameters the closed loop transfer function can be written as

$$G_{cq}(s) = \frac{i_q(s)}{i_{q,ref}(s)} = \frac{F_q(s)G'_q(s)}{1 + F_q(s)G'_q(s)} = \frac{\alpha_e\left(s + \frac{R+R_{aq}}{L_q}\right)}{\left(s + \alpha_e\right)\left(s + \frac{R+R_{aq}}{L_q}\right)}. \tag{4.16}$$

It can be seen that the closed loop system have one zero and two poles where one pole come from the process and the other pole from the controller. Furthermore, it can be seen that the controller pole is placed at $\alpha_e$ and that a pole and a zero cancels out. When active damping is added, the system pole and zero is moved to the control pole. Since both the zero and the pole is moved and they still cancel out, the dynamic behavior is not changed during ideal condition.

An anti wind-up algorithm was added to the current controller. It is needed since it always exists an upper limit in the voltage which is available for controlling the current. If the controller demands a voltage higher than the limit, the voltage is set to the upper voltage limit and the controller is unable to control the current. As is described in Section 4.1.1 this situation can lead to integrator windup which in this work is avoided by an anti wind-up algorithm. In Figure 4.2a and 4.2b it can be seen that the current can not be controlled when the voltage limit is reached at 57 ms and that there is an overshoot in current after 60 ms. In Figure 4.2bthe anti wind-up algorithm has been implemented and the current is controlled to the reference value without any overshoot after 60 ms. This indicates that the anti-windup strategy is working.

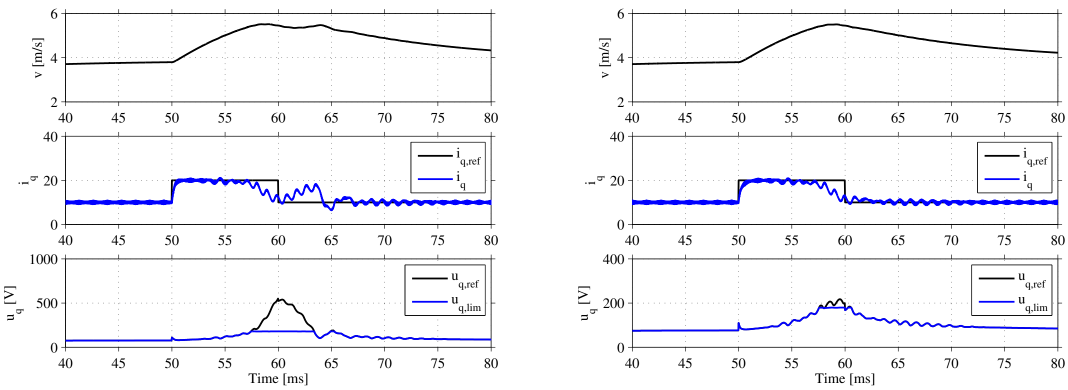


**(a)** A step in the current when the voltage limit is reached, without anti windup.

**(b)** A step in the current when the voltage limit is reached, with anti windup.

**Figure 4.2:** A step in the current when the voltage limit is reached. Behavior with and without anti windup strategy implemented.

### Current controller with parameter errors

In a real case it is impossible to have exact knowledge of the parameters used in the controller. In this section the current controller is evaluated when the estimated parameters used in the controller deviate from the real parameters in the machine.

In Figure 4.3 current step responses are simulated with the discrete time current controller, seen in (4.14), with different estimates of the inductance. In Figure 4.3a it is seen that the step response is closer to the ideal case if the inductance is overestimated compared to underestimated. This indicate that a slightly overestimation of the inductance is preferable instead of an underestimation. But in Figure 4.3b it is seen that too much overestimation can lead to instability. However, with a switching frequency of 20 kHz and $\alpha_e$ =5000 rad/s the inductance can be overestimated 6 times without giving an unstable current controller. The inductance is therefore still recommended to be slightly overestimated as long as it is carefully done.

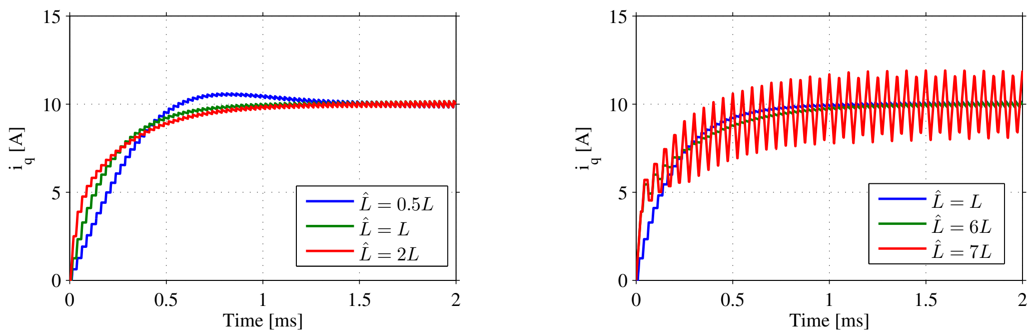


**(a)** Two times under- and overstimation of the stator inductance

**(b)** Large overestimation error of the stator inductance.

**Figure 4.3:** Current step response with estimation errors of $\hat{L}$

In Figure 4.4 the step responses are simulated with different estimates of the resistance. It is seen that current controller is much more robust against estimation errors of the resistance than of the inductance. This is since the active damping is much larger than the resistance in the stator windings. An estimated error of the resistance is therefore almost negligible compared to the total resistance used in the controller.

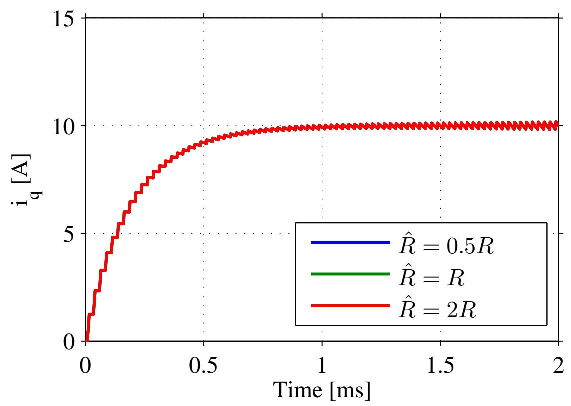


**Figure 4.4:** Estimation error in $\hat{R}$

# 5

# Rotor position and velocity observer

*Realization of the suggested control strategy depends on knowledge of the relative rotor position and speed. This knowledge can be acquired from mechanical sensors mounted in the machine. However, this will contribute to increased costs and reduction of mechanical robustness [24]. Due to this drawbacks, it is desirable to acquire the essential knowledge without these mechanical devices.*

*In general there exist two groups of sensorless control for permanent magnet synchronous machines. The first group is based on the induced back-EMF and the second on the possible magnetic saliency of the machine. In this chapter one approach from each of these groups are presented. The observer based on back EMF is called Statically Compensated Voltage Model (SCVM) and the observer based on magnetic saliency is in this work referred to as Square wave injection.*

## 5.1 Estimation based on the induced back-emf

Since the back-EMF is speed dependent, estimation techniques based on back-EMF has good performance in the medium and high speed range but is inaccurate for low and zero speed since the essential information they rely on then is lost [17]. This may sound unsuitable for an oscillating linear machine since zero speed is part of the working region. However, in this application energy will always be stored and returned between kinetic energy and potential energy in the gas springs. This means that the system will not need an accurate control at low speed to be accelerated and estimation techniques based on back-EMF could of that reason be of interest.

The statically compensated voltage model is a commonly used flux estimator for PMSM drives and is further described in [17]. The stator voltage in stationary coordinates can be written as

$$\mathbf{u}^s = R\mathbf{i}^s + \frac{d(L\mathbf{i}^s)}{dt} + \frac{d\mathbf{\Psi}^s}{dt} \tag{5.1}$$

where the time derivative also includes the inductance since it is a time dependent variable in stationary coordinates beacause of the magnetic saliency. The derivative of the rotor flux is equal to the back EMF. From (5.1) the rotor flux can be estimated as

$$\hat{\mathbf{\Psi}}^s = \int (\mathbf{u}_s^s - \hat{R}\mathbf{i}_s^s)dt - \hat{L}\mathbf{i}_s^s. \tag{5.2}$$

Equation (5.2) can not be used as it stands since it is marginally stable due to the integration. To gain stability the integration is substituted by a low pass filter which is obtained by adding a "leakage term" to (5.2),

$$\hat{\mathbf{\Psi}}^s = \int (\mathbf{u}_s^s - \hat{R}\mathbf{i}_s^s)dt - \hat{L}\mathbf{i}_s^s - \alpha_v \hat{\mathbf{\Psi}}^s. \tag{5.3}$$

The leakage term, $\alpha_v$, will introduce an error to the estimated flux which in steady state is given by

$$\hat{\mathbf{\Psi}}^s = \frac{j\omega_1}{j\omega_1 + \alpha_v}\mathbf{\Psi}^s, \tag{5.4}$$

where $\omega_1$ is the electrical frequency. It can be seen in (5.4) that the error between the estimated flux and the real flux is largest when the stator frequency is close to zero. Therefore a frequency dependency is introduced to the leakage term,

$$\alpha_v = \lambda|\omega_1|, \tag{5.5}$$

and the steady state error is compensated for so that the rotor flux estimation becomes

$$\hat{\mathbf{\Psi}}^s = \frac{1 - j\lambda sign(\hat{\omega}_1)}{s + \lambda|\hat{\omega}_1|}(\mathbf{u}^s - \hat{R}\mathbf{i}^s - \frac{d\hat{L}\mathbf{i}^s}{dt}). \tag{5.6}$$

In the rotating dq-system aligned with the rotor flux (5.6) becomes

$$\hat{\mathbf{\Psi}}^r = \frac{1 - j\lambda sign(\hat{\omega}_1)}{s + j\hat{\omega}_1 + \lambda|\hat{\omega}_1|}[\hat{e}_d - j\hat{e}_q], \tag{5.7}$$

where $\hat{e}_d$ and $\hat{e}_q$ are back emf in the d- and q-direction respectively. These are expressed as

$$\hat{e}_d = u_d - \hat{R}i_d + \hat{\omega}_1\hat{L}_q i_q - \hat{L}_d\frac{di_d}{dt} \tag{5.8a}$$

$$e_q = u_q - \hat{R}i_q - \hat{\omega}_1\hat{L}_d i_d - \hat{L}_q\frac{di_q}{dt}. \tag{5.8b}$$

The current derivatives is neglected due to the assumption that the current controller is much faster than the observer [17]. Equation (5.8) then becomes

$$\hat{e}_d = u_d - \hat{R}i_d + \hat{\omega}_1\hat{L}_q i_q \tag{5.9a}$$

$$\hat{e}_q = u_q - \hat{R}i_q - \hat{\omega}_1\hat{L}_d i_d. \tag{5.9b}$$

The magnitude of the rotor flux is known in a PMSM since it is dependent on the chosen magnets. The speed can thus be calculated from the imaginary part of (5.7) as

$$\hat{\omega}_1 = \frac{\hat{e}_q - \lambda sign(\hat{\omega}_1)\hat{e}_d}{\hat{\Psi}_{PM}}. \tag{5.10}$$

An algebraic loop is present in (5.10) since the speed is needed to calculate $\hat{e}_d$ and $\hat{e}_q$. This is solved with a low pass filter. As long as the bandwidth of the filter is higher than the dynamics of the mechanical system the filtration do not affect the estimation. The SCVM in dq-coordinates is thus written as

$$\dot{\hat{\omega}}_1 = \alpha\left(\frac{\hat{e}_q - \lambda sign(\hat{\omega}_1)\hat{e}_d}{\hat{\Psi}_{PM}} - \hat{\omega}_1\right) \tag{5.11a}$$

$$\dot{\hat{\theta}} = \hat{\omega}_1, \tag{5.11b}$$

where $\alpha = \alpha_0 + 2\lambda|\hat{\omega}_1|$ is the bandwidth of the low pass filter chosen from the recommendations in [25]. In the same way as the current controller, the observer is discretized by the forward Euler approximation, seen in (4.13). A discrete version of (5.11) is obtained as

$$\hat{\omega}_{1,k+1} = \hat{\omega}_{1,k} + \alpha T\Big(\frac{\hat{e}_{q,k} - \lambda sign(\hat{\omega}_{1,k})\hat{e}_{d,k}}{\hat{\Psi}_{PM}} - \hat{\omega}_{1,k}\Big) \tag{5.12a}$$

$$\hat{\theta}_{k+1} = \hat{\theta}_k + T\hat{\omega}_{1,k}. \tag{5.12b}$$

### 5.1.1 Evaluation of the SCVM

The evaluation is performed with the discrete version of the SCVM seen in (5.12) with a switching frequency of 20 kHz. A current step with an amplitude of 10

A is applied in the q-direction which causes the relative speed between rotor and stator to increase as a first order system. The current step and the relative speed is plotted in Figure 5.1. The speed reaches 460 rad/s after 30 milliseconds.

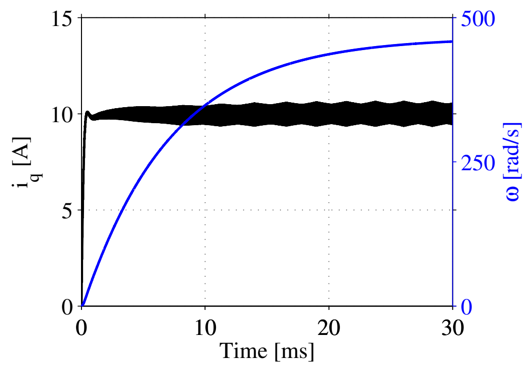


**Figure 5.1:** Current step applied to the TLPMSM and the speed response.

The tuneable parameters of the SCVM are the bandwidth of the low pass filter, $\alpha_0$, and the leakage term, $\lambda$. The influence of $\lambda$ is seen in Figure 5.2 where the error between the estimated position and the actual position is plotted in the top graph and the error between the estimated speed and the actual speed is plotted in the bottom graph. A positive value means that the estimation lags the actual value. It is seen that a higher $\lambda$ gives a faster convergence to the correct estimation. It is also seen that the speed estimation leads the actual value in the first millisecond, due to the neglection of the current derivative in (5.9), and that this error is greater with higher $\lambda$.

In Figure 5.3 the influence of $\alpha_0$ is seen. It is seen that the behavior is similar to that of $\lambda$ in the sense that a higher $\alpha_0$ gives faster convergence to the correct estimation and higher impact of the neglected current derivative. This is intuitive since $\alpha_0$ is the bandwidth of the low-pass filter used to break the algebraic loop. A higher value of $\alpha_0$ reduce the low-pass effect and in that sense also reduce the influence on the estimation.

### Statically compensated voltage model with parameter errors

The tuneable paramaters are chosen as $\alpha_0 = 1000$ rad/s and $\lambda = 2$. The other parameters used in the SCVM are the estimation of the stator resistance, stator inductance in d- and q-direction and the rotor flux.

It can be seen in (5.9) that the terms involving the estimation of the resistance is proportional to the current and the term involving the inductance is both proportional to the current and the relative speed between the rotor and stator. This means that the estimation of the resistance is more important to the performance

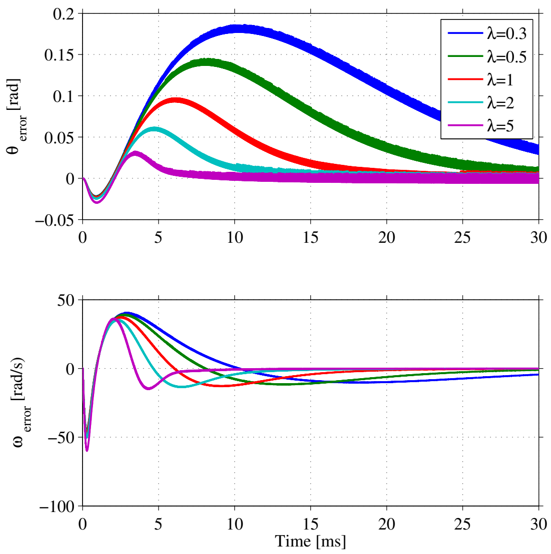


**Figure 5.2:** Position estimation error and speed estimation error for the SCVM when $\alpha_0$=1000 and $\lambda$ is swept from 0.5 to 5.

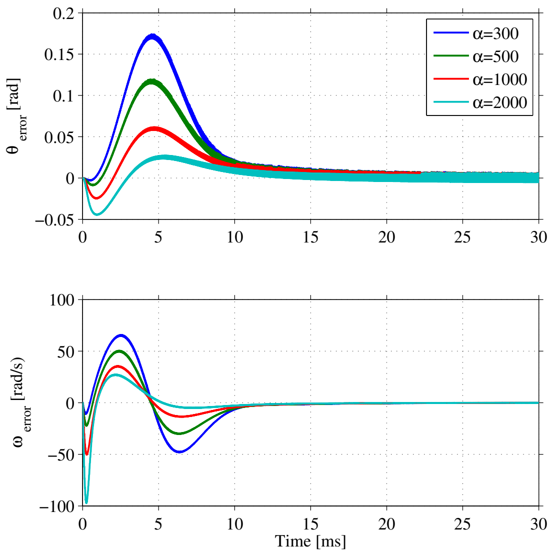


**Figure 5.3:** Position estimation error and speed estimation error for the SCVM when $\lambda$=2 and $\alpha_0$ is swept from 300 to 2000.

of the observer when the current is high and the speed is low since the voltage over the resistance then is a larger part of the estimated back-EMF. For the same reasons, the estimation of the inductance is more important to the performance of the observer when the product between the current and the relative speed is high.

The sensitivity to estimation errors is, for this reason, dependent on under which conditions the SCVM is tested.

In this evaluation, simulations are made under the same conditions as shown in Figure 5.1. In Figure 5.4 the position estimation error and the speed estimation error are seen for different estimations of the stator inductance. It can be seen that the observer is unable to put the position estimation error to zero for all errors in the inductance estimation. The error in the position estimation does not exceed 0.1 radians even with 2 times overestimation and 5 times underestimation. Since the steady state for an oscillating linear machine is not the same as for a rotating machine, the inductance estimation is not as important in this application as it is for a rotating machine. It will therefore be slightly overestimated due to the recommendations for the current controller.

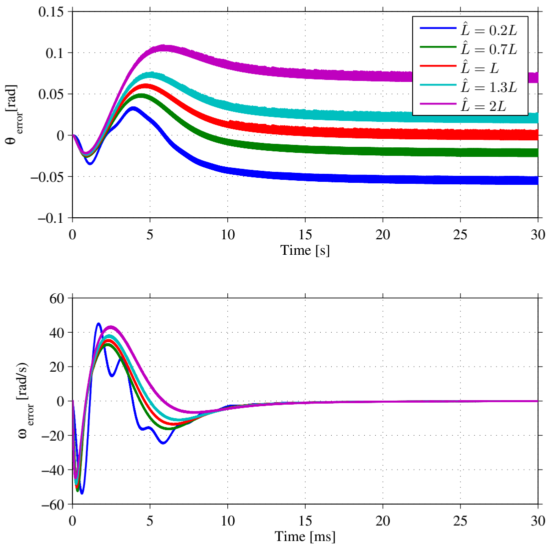


**Figure 5.4:** Estimation error in rotor position and speed when the estimated inductance used in the SCVM deviates from the real inductance. $\alpha_0$ =1000 rad/s, $\lambda = 2$

The same simulation is made for different estimations of the resistance and the rotor flux. In Figure 5.5 it can be seen that the SCVM is very robust against errors in the resistance estimation. The errors are almost identical even with 2 times overestimation and 5 times underestimation. In Figure 5.6 it can be seen that the estimation of the motor flux is very important to the SCVM. Fairly small errors in the rotor flux estimaion directly generate error in the position estimation. It should also be noted that the SCVM estimates the speed correctly in steady state even with high parameter errors.

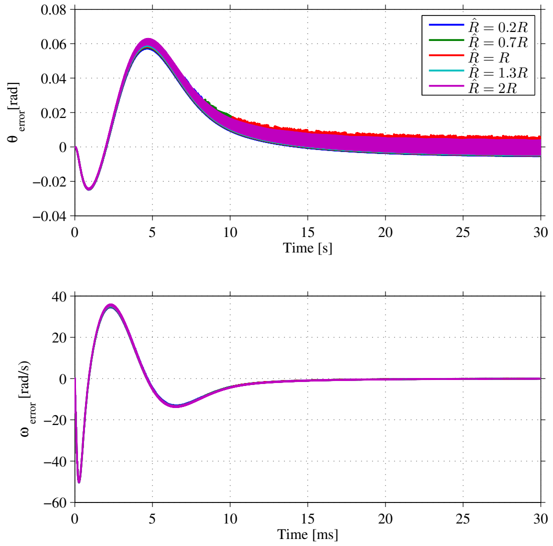


**Figure 5.5:** Estimation error in rotor position and speed when the estimated resistance used in the SCVM deviates from the real resistance. $\alpha_0$ =1000 rad/s, $\lambda = 2$

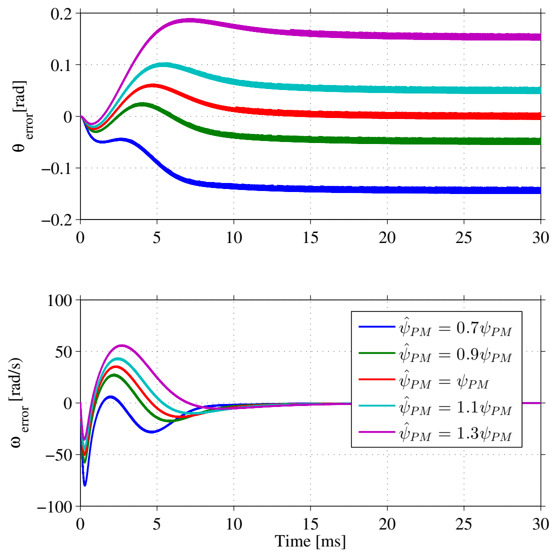


**Figure 5.6:** Estimation error in rotor position and speed when the estimated motor flux constant used in the SCVM deviates from the real motor flux constant. $\alpha_0$ =1000 rad/s, $\lambda = 2$

## 5.2 Estimation based on square wave injection

A fundamental condition for estimation techniques based on signal injection is that the machine must be salient, which in this context means different inductance in d-and q-direction [24]. Saliency is common for permanent magnet machines with the magnets mounted inside the iron of the rotor. Those machines are often referred to as interior permanent magnet synchronous machines, IPMSMs. The saliency is generated by the different magnetic properties for iron and permanent magnets [24]. There are several different estimation techniques based on high frequency signal injection presented in literature. Some of these inject a signal in the $\alpha\beta$-reference frame and are called rotating injection. Others inject a signal either on the d-axis or the q-axis and are called pulsating injection [26]. The most well-known method was proposed in [27] and uses a rotating sinusoidal voltage injection. To extract the information of the rotor position the high frequency current need to be seperated from the fundamental current, this was done with a low pass filter and a band pass filter [27]. However, these filters degrade the dynamic performance of the control system because of the inevitable time delay. This limits the bandwidth of the speed control up to a few Hertz [28].

The approach used in this work was proposed in [24] where it is also described in more detail. The main idea is to inject a square wave shaped, high frequency voltage in the assumed d-direction and then look at the current response in both the assumed d- and q-direction. The response can be used to acquire a signal proportional to the error between the assumed and the correct orientated rotor flux. The error signal is then used as input to a Phase Locked Loop (PLL) to track the position and speed of the rotor. The main advantage of using a square wave shape instead of a sinusoidal wave shape is that it could be coordinated with the sampling which means that the information can be extracted without filters [28]. This also gives the possibility of using a injected signal with a higher frequency compared to when a sinusoidally shaped injected voltage is used, which improves the dynamical performance of the observer [24].

If the frequency of the injected voltage is selected sufficiently high the electrical system will be dominated by the term involving the derivative in (3.8). Moreover, the derivative is approximated to visualize the current ripple. Equation (3.8) then reduces to

$$\begin{bmatrix} u_d \\ u_q \end{bmatrix} = \begin{bmatrix} L_d & 0 \\ 0 & L_q \end{bmatrix} \frac{1}{T/2} \begin{bmatrix} \Delta i_d \\ \Delta i_q \end{bmatrix}. \tag{5.13}$$

The high frequency square wave signal is injected in the d-direction of the estimated rotor reference frame and can be expressed as

$$U_{inj} = \begin{cases} U_h & \text{if } 0 < t \leq \frac{T}{2} \\ -U_h & \text{if } \frac{T}{2} < t \leq T. \end{cases} \tag{5.14}$$

The reference frame can of course deviate from the real rotor reference frame. The injected voltage in the real reference frame can be expressed as

$$U_{dq} = \pm U_h \begin{bmatrix} cos\tilde{\theta} \\ -sin\tilde{\theta} \end{bmatrix} \tag{5.15}$$

where $\tilde{\theta}$ is the error between the real and estimated rotor reference frame. Combining (5.13) and (5.15) gives

$$\begin{bmatrix} \Delta i_d \\ \Delta i_q \end{bmatrix} = \pm U_h \cdot \frac{T}{2} \begin{bmatrix} \frac{1}{L_d} cos\tilde{\theta} \\ \frac{-1}{L_q} sin\tilde{\theta} \end{bmatrix}. \tag{5.16}$$

When the current ripple is measured it can only be done in the estimated reference frame. If (5.16) is transformed to the estimated reference frame the expression becomes

$$\begin{bmatrix} \Delta \hat{i}_d \\ \Delta \hat{i}_q \end{bmatrix} = \pm U_h \cdot \frac{T}{2} \begin{bmatrix} \frac{cos^2\tilde{\theta}}{L_d} + \frac{sin^2\tilde{\theta}}{L_q} \\ \frac{1}{2}\left(\frac{1}{L_d} - \frac{1}{L_q}\right) sin2\tilde{\theta} \end{bmatrix}. \tag{5.17}$$

From (5.17) it can be seen that the ripple in q-direction contains information about the rotor position.

In the motor the current ripple consists of two parts, the ripple calculated in (5.17) which is generated by the injected voltage and the ripple generated by the current control voltage. Only the ripple generated by the injected voltage is useful for the position estimation and only this part should be used for determining the rotor flux position. To extract this part of the current ripple from the current measurement, the injected square wave is synchronized to the sampling as is seen in Figure 5.7a. It can be seen that the sampling is coordinated with the peaks of the current ripple generated by the injected voltage and with the average value of the current ripple generated by the current control voltage. In Figure 5.7b the current in d- and q-direction is seen when the square wave voltage is injected ideally in the real rotating reference frame. It is assumed that the slope of the current generated by the current control voltage is constant since the discrete current controller only updates the voltage reference once each sampling period.

With a non-ideal estimated flux angle, the injected voltage in the assumed d-direction will affect the real q-direction as is seen in (5.17). The current ripple in d- and q-direction generated by the injected voltage is then calculated as follows

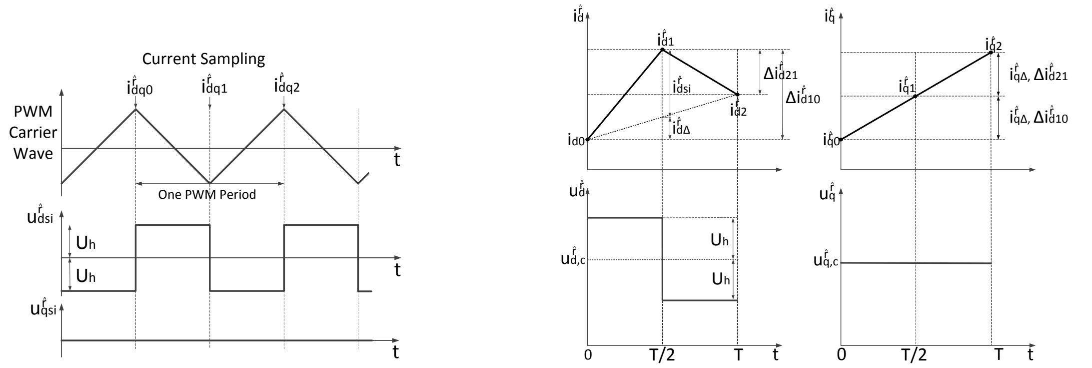


**(a)** Sampling of current is synchronized with the injected voltage.

**(b)** Current ripple created by the injected voltage.

**Figure 5.7:** The sampling of the current and the ripple created by the injected voltage.

$$\Delta i^{\hat{r}}_{d10} = i^{\hat{r}}_{d1} - i^{\hat{r}}_{d0} = i^{\hat{r}}_{d\Delta} + i^{\hat{r}}_{dsi} \tag{5.18a}$$
$$\Delta i^{\hat{r}}_{q10} = i^{\hat{r}}_{q1} - i^{\hat{r}}_{q0} = i^{\hat{r}}_{q\Delta} + i^{\hat{r}}_{qsi} \tag{5.18b}$$
$$\Delta i^{\hat{r}}_{d21} = i^{\hat{r}}_{d2} - i^{\hat{r}}_{d1} = i^{\hat{r}}_{d\Delta} - i^{\hat{r}}_{dsi} \tag{5.18c}$$
$$\Delta i^{\hat{r}}_{q21} = i^{\hat{r}}_{q2} - i^{\hat{r}}_{q1} = i^{\hat{r}}_{q\Delta} - i^{\hat{r}}_{qsi} \tag{5.18d}$$

$$\Rightarrow \begin{bmatrix} i^{\hat{r}}_{dsi} \\ i^{\hat{r}}_{qsi} \end{bmatrix} = \frac{1}{2}\begin{bmatrix} \Delta i^{\hat{r}}_{d10} - \Delta i^{\hat{r}}_{d21} \\ \Delta i^{\hat{r}}_{q10} - \Delta i^{\hat{r}}_{q21} \end{bmatrix} = T \cdot U_{inj} \begin{bmatrix} \frac{cos^2(\tilde{\theta}_r)}{L_d} + \frac{sin^2(\tilde{\theta}_r)}{L_q} \\ \left(\frac{1}{L_d} - \frac{1}{L_q}\right) sin2\tilde{\theta}, \end{bmatrix} \tag{5.19}$$

where 0, 1 and 2 stands for different samples.

In [24] the error angle is extracted by the use of two orthogonal measurement axes denoted $d^m$ and $q^m$. The measurement axes are phase shifted $\frac{\pi}{4}$ from the ordinary dq-system. In this coordinate system the current ripple is expressed as

$$\begin{bmatrix} i^{\hat{m}}_{dsi} \\ i^{\hat{m}}_{qsi} \end{bmatrix} = T_{-\frac{\pi}{4}} \begin{bmatrix} i^{\hat{r}}_{dsi} \\ i^{\hat{r}}_{qsi} \end{bmatrix} = \pm \frac{T \cdot U_h}{2\sqrt{2}} \begin{bmatrix} \frac{cos^2(\tilde{\theta}_r)}{L_d} + \frac{sin^2(\tilde{\theta}_r)}{L_q} - \frac{1}{2}\left(\frac{1}{L_d} - \frac{1}{L_q}\right) sin2\tilde{\theta} \\ \frac{cos^2(\tilde{\theta}_r)}{L_d} + \frac{sin^2(\tilde{\theta}_r)}{L_q} + \frac{1}{2}\left(\frac{1}{L_d} - \frac{1}{L_q}\right) sin2\tilde{\theta} \end{bmatrix} \tag{5.20}$$

By assuming small errors, the error angle between the assumed and real dq-system can be obtained from (5.20) as

$$\epsilon = \tilde{\theta} = \frac{\sqrt{2}\hat{L}_d\hat{L}_q}{(\hat{L}_q - \hat{L}_d)T \cdot U_h}\left(|i_{qsi}^{\hat{m}}| - |i_{dsi}^{\hat{m}}|\right) \tag{5.21}$$

The orientation of the estimated reference frame is then obtained by using the error signal as input to a phase locked loop (PLL) which is described by the following equations

$$\dot{\hat{\omega}} = \gamma_1\epsilon \tag{5.22a}$$

$$\dot{\hat{\theta}} = \hat{\omega} + \gamma_2\epsilon, \tag{5.22b}$$

where $\gamma_1$ and $\gamma_2$ are gain parameters. It can be noted that $\hat{\theta}$ is the integral of $\hat{\omega}$ but with a correction term. Assuming that the error is small, $\hat{\theta} \approx \theta$ the PLL can be linearized as

$$\dot{\hat{\omega}} = \gamma_1(\theta - \hat{\theta}) \tag{5.23a}$$

$$\dot{\hat{\theta}} = \hat{\omega} + \gamma_2(\theta - \hat{\theta}). \tag{5.23b}$$

This render in the characteristic polynomial $s^2 + \gamma_2 s + \gamma_1$. Both the poles are placed at $s = -\rho$ by selecting $\gamma_1 = \rho^2$ and $\gamma_2 = 2\rho$, where $\rho$ is the bandwidth of the PLL [29]. The PLL is discretized with the forward Euler approximation and discrete version of (5.22) is obtained as

$$\hat{\omega}_{k+1} = \hat{\omega}_k + T\gamma_1\epsilon_k \tag{5.24a}$$

$$\hat{\theta}_{k+1} = \hat{\theta}_k + T\hat{\omega}_k + T\gamma_2\epsilon_k. \tag{5.24b}$$

### 5.2.1 Evaluation of Square wave injection

The tuneable parameters are the amplitude ($U_h$), the frequency ($f_h$) of the injected signal and the bandwidth ($\rho$) of the PLL. The frequency is chosen to be the highest possible, which is the same as the switching frequency, 20 kHz.

All simulations in this section are performed when a current step with an amplitude of 10 A is applied in the q-direction, as is seen in Figure 5.1. The relative angular speed between rotor and stator increases as a first order system and reaches 460 rad/s after 30 milliseconds. In Figure 5.8 the result of the simulation is seen when the amplitude of the injected signal is swept between 10 V to 80 V. It is seen that the position and speed errors are smaller in the first few milliseconds for higher amplitudes. But that all amplitudes gives a steady state error in the position estimation. The reason for the steady state error could not be explained. In

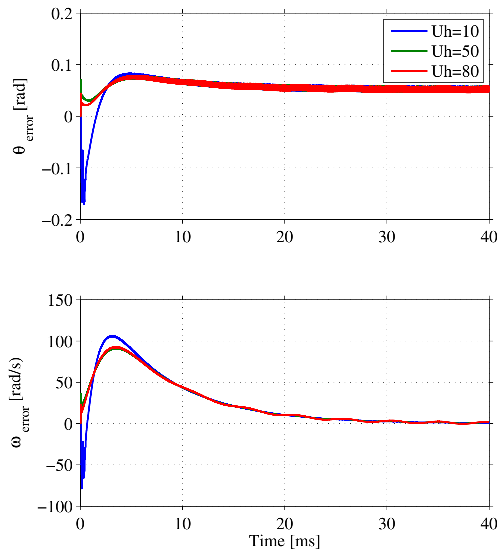


**Figure 5.8:** Position and speed error with the square wave injection technique. $U_h$=10 V-80 V, $\rho$=1000.

experimental tests in [24] a steady state error is explained with flux saturation. The speed error is reduced to zero after 30 milliseconds for all the simulated amplitudes.

In Figure 5.9 different values for the bandwidth of the PLL is simulated. As expected, it is seen that a higher bandwidth gives a faster convergence of the estimated position and speed. Furthermore, it is seen that higher bandwidths give higher error in the first millisecond for both the relative position and speed. This is since higher bandwidths react more on the current derivative, see the current response in Figure 5.1 and compare to Figure 5.9. Since successive current samples are compared, the current from the control voltage cancels out if the current derivative is low, which it is not in the first millisecond. If the bandwidth is high the estimation is more sensitive to current derivatives.

### Square wave injection with parameter errors

The only parameters which need to be estimated are the inductance in d- and q-direction which are used to normalize the error signal, seen in (5.21). Simulations are made in the same scenario as previously and the estimated inductance value in d- and q-direction are changed proportionally. The result is seen in Figure 5.10 where an underestimation of the inductance gives a slower estimation and overestimation a faster estimation. An overestimation of the inductance also gives more sensitivity to the current derivative. This means that the inductance estimation basically only affects the bandwidth of the PLL.

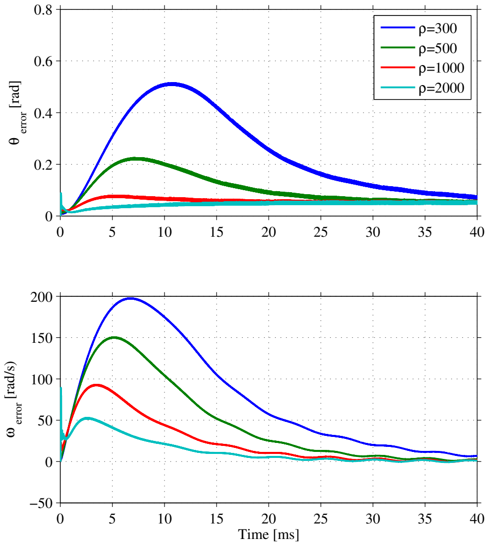


**Figure 5.9:** Position and speed error with the square wave injection technique. $U_h$=80 V, $\rho$=300-2000.

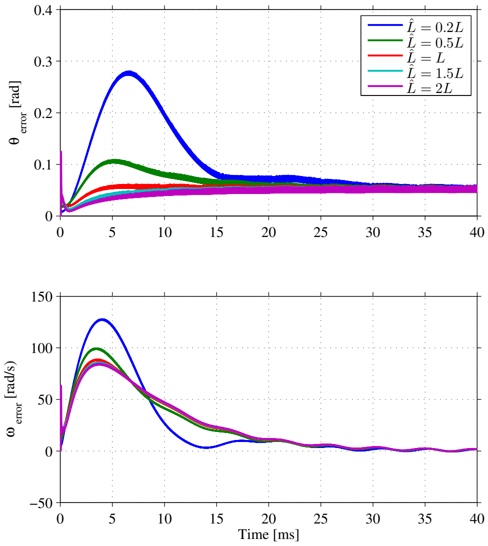


**Figure 5.10:** Value of the inductance estimation swept from 0.2 to 2 times of the actual value. Position and speed error with the square wave injection technique. $U_h$=80 V, $\rho$=1000.

A possible problem for the Square Wave Injection implemented in a real drive system is the start up. Since the saliency is identical for every pole pair it is possible for the PLL to be locked 180°out of phase [24]. However, in this application the support springs seen in Figure 2.1 are used to make the machine start from the same position every time.

# 6

# Control Strategy

*The aim of this chapter is to present the control strategies used to oscillate the Resonator such that the mass attached to the stator can be used as a hammer to crush rocks. First an open loop strategy is presented and then a closed loop strategy. The closed loop strategy is then analysed in an ideal situation with perfectly estimated/measured signals and then with the observers presented in Chapter 5.*

## 6.1 Open loop control

An easily designed control system is obtained by using an open loop oscillation controller. The mechanical system can be oscillated by selecting a force reference with a selectable frequency, as is seen in Figure 6.1. The relative speed between the rotor and stator will have the same frequency as the current in the q-direction which is proportional to the output force from the electrical system. The problem is to select the frequency of the force reference as the resonance frequency of the mechanical system, since the resonance frequency is dependent on process parameters.

The resonance frequency can be determined by changing the frequency of the force reference and observing the response of the relative displacement between the rotor and stator. The amplitude of the oscillations of the relative displacement between the rotor and stator has a maximum at the resonance frequency. To maintain the oscillations at resonance frequency the process must be observed and tuned during operation.

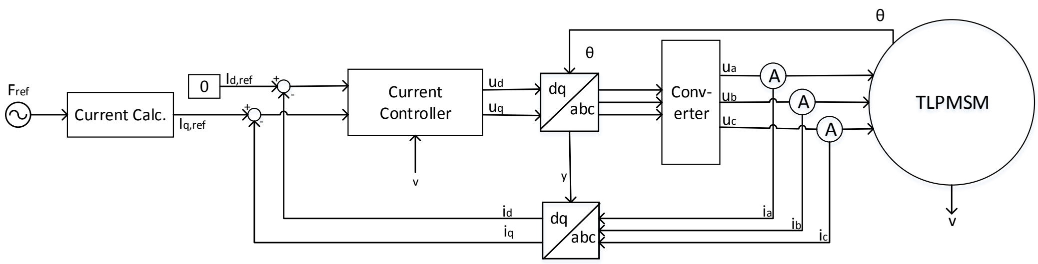


**Figure 6.1:** A block diagram showing the control system with open loop oscillation control.

## 6.2 Closed loop control

The power supplied to the mechanical system from the electrical system is

$$P = F_e v \tag{6.1}$$

where $v$ is the relative motion between the piston and the casing and $F_e$ is the force which is proportional to the current in q-direction. From (6.1) it can be concluded that there should not be a current in the stator windings if the relative motion is zero because it would not contribute to any output power, only generate copper losses. It is also important that the power is positive so the oscillation is not damped which means that the current applied to the machine should always have the same sign as the relative motion. Furthermore, it is desirable to have a control system which works for different types of rocks and process parameters which will generate different resonance frequencies for the system.

The oscillation are controlled by a proportional controller with positive feedback of the relative speed between the rotor and the stator. The output from this controller is the reference to the force controller. Since the feedback is positive the system will be unstable, but the behavior is exactly what is wanted. The force will always have the same sign as the relative motion and when the relative motion is zero, the force is zero. This also means that the force and the relative speed will have the same frequency, and the force is applied at the resonance frequency.

But if the energy supplied from the electric motor is not limited, the stroke length will increase until, sooner or later, the machine breaks. Therefore, a condition is inserted to the controller. If the relative displacement between the piston and casing is too large the reference to the force controller should be set to zero. This condition limits the energy supplied from the electric motor to the mechanical system.

An overview of the control scheme is seen in Figure 6.2 where the Oscillation controller described in this section consists of the two blocks "Proportional gain" and "Force Limitation". The output from this controller is calculated to be a current reference with (3.10), which is used as input to the current controller described in Chapter 4.

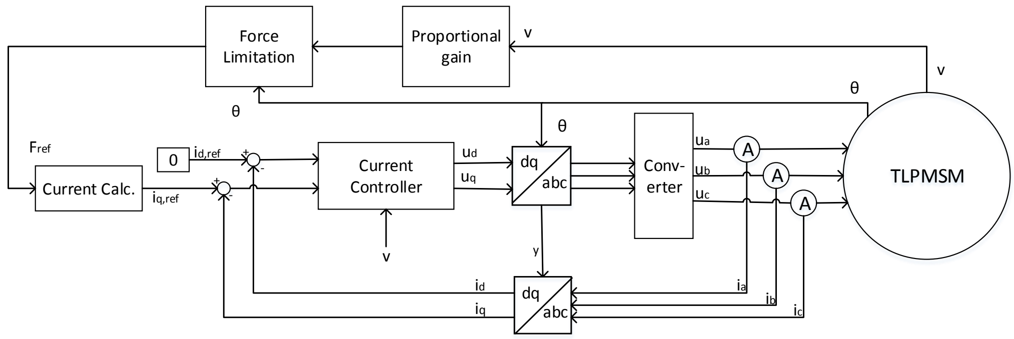


**Figure 6.2:** A block diagram showing the closed loop control system.

In Figure 6.3 it can be seen that with this type of control system the electrical force, which is proportional to the q-current, is applied when the relative speed is high. This means that it is current in the windings only when the TLPMSM is able to produce output power, see (6.1). This prevents unnecessary copper losses.

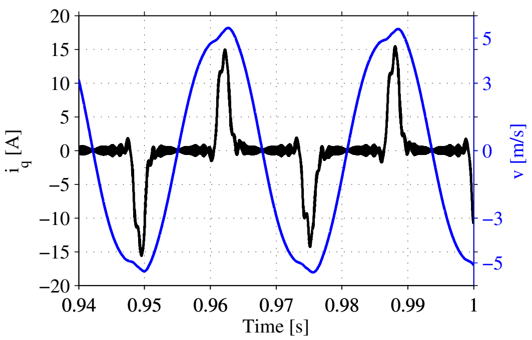


**Figure 6.3:** A current is only applied when there is a relative speed between the piston and the casing. The current is also applied with the same sign and frequency as the relative speed.

### 6.2.1 Evaluation of Oscillation controller

The tunable parameters in the oscillation controller are the proportional gain and the force limitation. The proportional gain and the force limitation both control the energy injected to the system in each oscillation. Higher gain give a higher reference current which means that higher peak force is applied to the rotor, which in turn give higher oscillations. The force limitation is controlling how long distance of the oscillation that force is applied. In Figure 6.4 the electric force together with the force reference are plotted versus the relative displacement between casing and piston. The dashed area under the blue curve represents the injected energy in one oscillation cycle and it is seen that both the force reference and the limit determine the injected energy. The oscillations reach steady state when the injected energy is balanced by the losses and the impact energy to the rock.

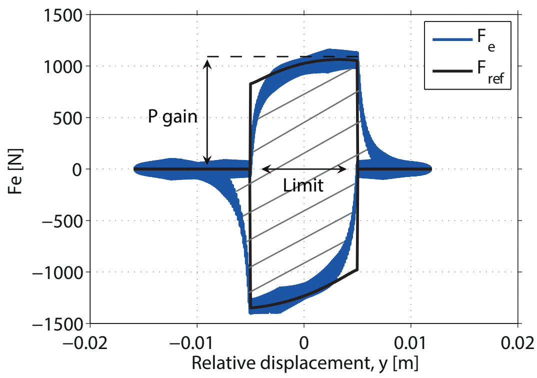


**Figure 6.4:** The electric force and its reference versus relative displacement between casing and piston.

The top force or weight on bit is also an available control parameter. It pushes the Resonator down towards the rock surface and is denoted $F_{WOB}$ in Figure 3.7. To get even and hard strokes this parameter need to be tuned during the operation of the Resonator since it is affected by the rock properties and the other two control parameters. In Figure 6.5 it can be seen that the weight on bit should be between 100 N and 900 N for a certain wroking condition. With a lower top force than 100 N the Resonator will only bounce on the rock surface and a higher top force than 900 N will cause the Resonator to hit the rock in non-ideal time instants. Even higher top force will eventually choke the oscillations completely. It should be stressed that the relationship between the top force and the impact force seen in Figure 6.5 is for a specific working condition. Thus it only gives a hint about how critical the control of the top force is for the operation of the Resonator.

In Figure 6.6 the complete behavior of the system is seen with the oscillation controller in steady state . The control parameters are selected as $P = 400$ Ns/m,

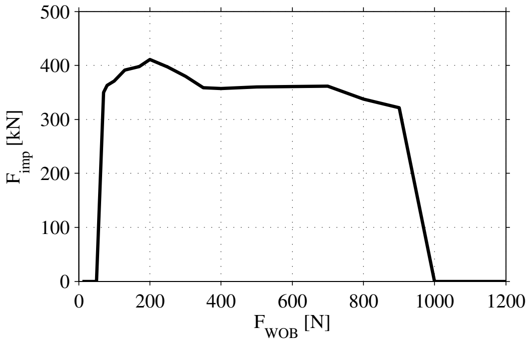


**Figure 6.5:** The impact force (F$_{imp}$) versus applied top force (F$_{WOB}$).The other control parameters are selected as $P = 400$ Ns/m, $limit = 5$ mm.

$limit = 5$ mm and $F_{WOB} = 200$ N. The oscillation frequency can be calculated to about 38 Hz and it is seen that the rock is hit every second oscillation. The impact force to the rock is denoted $F_{rock}$ and it reaches 400 kN each hit. It can also be seen that the relative position between piston and casing, denoted x, is less than 30 mm. It can be recalled from the construction of the Resonator presented in Section 2.2 that there are 14 poles in the piston. If the relative position is kept within 30 mm, which is the length of two pole pitches, there is always 10 active poles. This ensures a good utilization of the stator current and the rotor flux. The $i_q$ current reaches 10 A and it is applied at the peak of the relative speed between piston and casing.

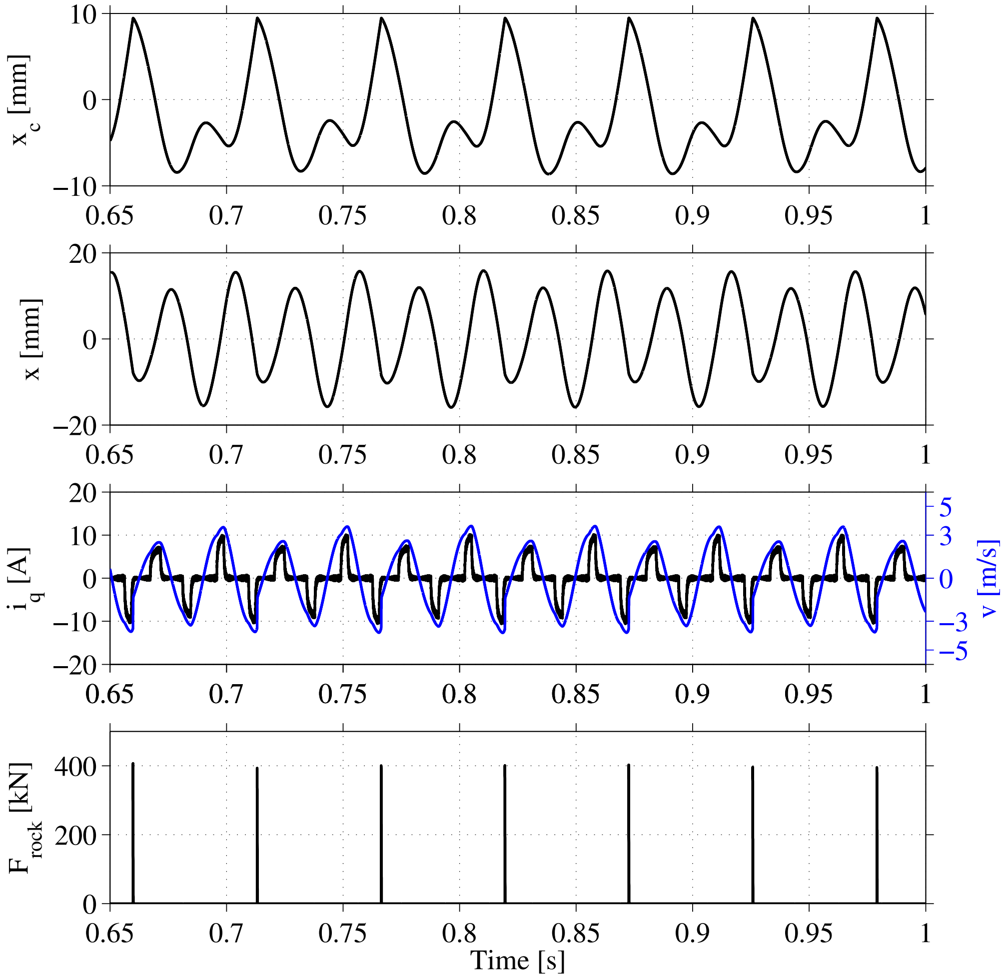


**Figure 6.6:** Behavior of complete system with oscillation control. The control parameters are selected as $P = 400$ Ns/m, $limit = 5$ mm and $F_{WOB} = 200$ N.

As was seen in Figure 6.4, the injected energy in to the mechanical system is dependent on the values of the proportional gain and the limit. In Figure 6.7 the impact force to the rock is seen for different values of force limitation and proportional gain. It can be seen that higher values for both the control parameters give more energy to the mechanical system and in turn higher impact force to the rock. It is also seen that a larger limit than 10 mm in Figure 6.7a and a larger proportional gain than 700 Ns/m in Figure 6.7b give lower or almost no higher impact force. This is since the voltage limit is reached when the oscillation controller demands current.

In Figure 6.8 the proportional gain and the limit are selected so high that the voltage limit at 180 V is reached when the relative speed is high. It can be seen

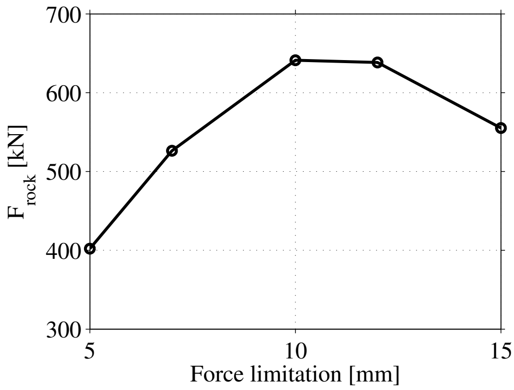


**(a)** Impact force to the rock versus different force limitation. $P = 400$ Ns/m and $F_{WOB} = 200$ N.

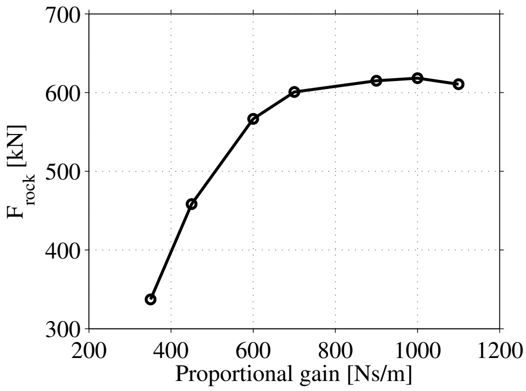


**(b)** Impact force to the rock versus different proportional gain. $limit = 5$ mm $F_{WOB} = 200$ N.

**Figure 6.7:** Impact force to the rock versus different proportional gain and force limitation.

that when the voltage limit is reached the current gets uncontrolled and do not respond like a first order system. It is also seen that the rock is hit every second oscillation and that the relative position still is less than two pole pitches. The impact force is 645 kN with the same frequency as in Figure 6.6.

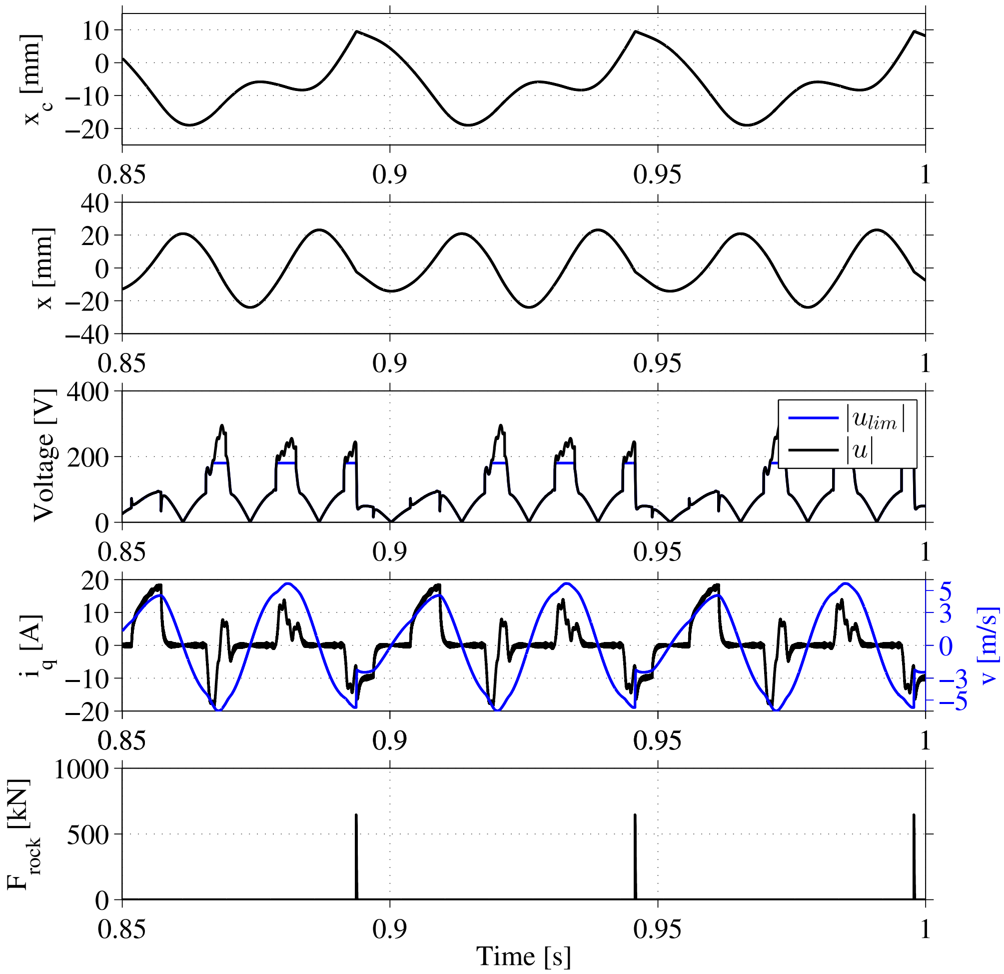


**Figure 6.8:** Behavior of complete system with oscillation control. The control parameters are selected as $P = 600$ Ns/m, $limit = 10$ mm and $F_{WOB} = 200$ N.

### 6.2.2 Evaluation of Oscillation controller with SCVM

In the evaluation of SCVM the parameters are selected as $\alpha_0 = 1000$ rad/s, $\lambda = 2$ and $\hat{L} = 0.9L$. The control parameters are selected to be the same as was used in Figure 6.6, $P = 400$ Ns/m, $limit = 5$ mm and $F_{WOB} = 200$ N. In Figure 6.9 the complete behavior is seen when the SCVM is used to estimate the relative position and speed between rotor and stator. It is seen that the behavior is similar to when perfect measurements of relative position and speed was used, seen in Figure 6.6. The impact force to the rock reaches 417 kN which is higher than in Figure 6.6 since the speed is slightly overestimated the force reference becomes higher. The oscillation frequency is the same as in Figure 6.6. In the third graph from the top, the error between actual and estimated relative position is plotted. It can be seen that the error is always below 2 mm or 10 % of the actual position.

To show that the SCVM is insensitive to noise a high amount of uncorrelated gaussian noise was added to the phase current measurements. The noise was added in Simulink with the block diagram seen in Figure 6.11 with the variance of the "random number"-blocks set to 10% of the measured values. In the fourth graph from the top in Figure 6.9, it can be seen that the current controller is affected by the added noise but that the q-current is still applied at the correct time instants and with roughly the desired amplitude. This is showing that the SCVM is insensitive to measurement noise.

In Figure 6.10 the SCVM is simulated in the same situation as in Figure 6.9 but with parameter errors. The used parameters are $\hat{\Psi} = 0.8\Psi$, $\hat{L}_d = 0.8L_d$, $\hat{L}_q = 0.8L_q$ and $\hat{R} = 0.8R$ which also are used for the current controller. It can be seen that the impact from current derivative is larger compared to Figure 6.9 and this also influence the position error. Despite this, the q-current is applied when the relative speed between the rotor and stator is high and the impact force to the rock is 343 kN.

One of the tunable parameters in the SCVM is the leakage term, $\lambda$, as was selected $\lambda = 2$ in the evaluation above. The leakage term was added to gain stability by approximate the integration in the SCVM as a lowpass filter. This means that a large value of $\lambda$ makes the SCVM faster but also more sensitive to disturbances, as for example the current derivative. In Figure 6.12 two simulations are seen with two different values of $\lambda$. It can be seen that when $\lambda = 5$ is used the SCVM is much more affected by the current derivative than when $\lambda = 2$ is used.

A drawback of the SCVM is that the method is based on the induced back EMF which is proportional to the speed. Therefore the initial relative position can not be estimated which can be a problem when the SCVM is implemented in a real drive system [25].

### 6.2.3 Evaluation of Oscillation controller with square wave injection

A number of simulations were performed on the complete electromechanical system to evaluate the trade off between the choice of observer parameters when using the Square Wave Injection technique. In a real world system there will be measurement noise and this observer need to be able to distinguish the high frequency signal from the noise. Current measurement noise was added with the blocks seen in Figure 6.11 and the noise level is altered by changing the variance of the "random number"-blocks. In Figure 6.13a it is seen how much measurement noise the observer can handle for different amplitude of the injected square wave voltage with $\rho$=500

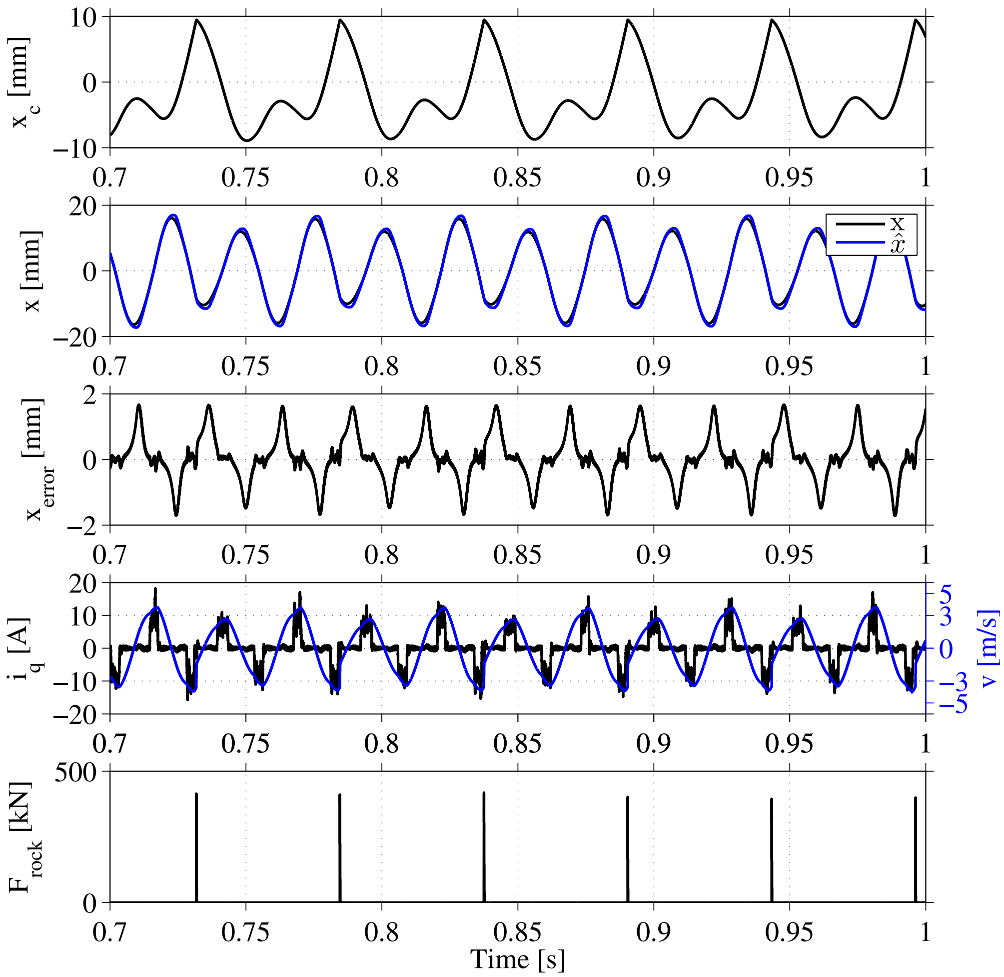


**Figure 6.9:** Behavior of complete system with oscillation control and SCVM. The control parameters are selected as $P$ = 400 Ns/m, $limit$ = 5 mm and $F_{WOB}$ = 200 N. The parameters for the SCVM are selected as $\alpha_0$ = 1000 and $\lambda$ = 2. 10% measurement noise added.

rad/s when the Resonator is moved without hitting the rock. As can be expected, the observer can handle higher measurement noise when using higher amplitude of the injected voltage.

Since the field orientation is not always correct the injected voltage in the d-direction will create a ripple in the force producing q-current, and consequently generate a ripple in the force. In Figure 6.13b the peak to peak force ripple is seen for different amplitude of the injected signal with $\rho$=500 rad/s when the Resonator is moved without hitting the rock. The ripple in the force is increasing with higher amplitude which will cause extra wear and losses in the machine. From

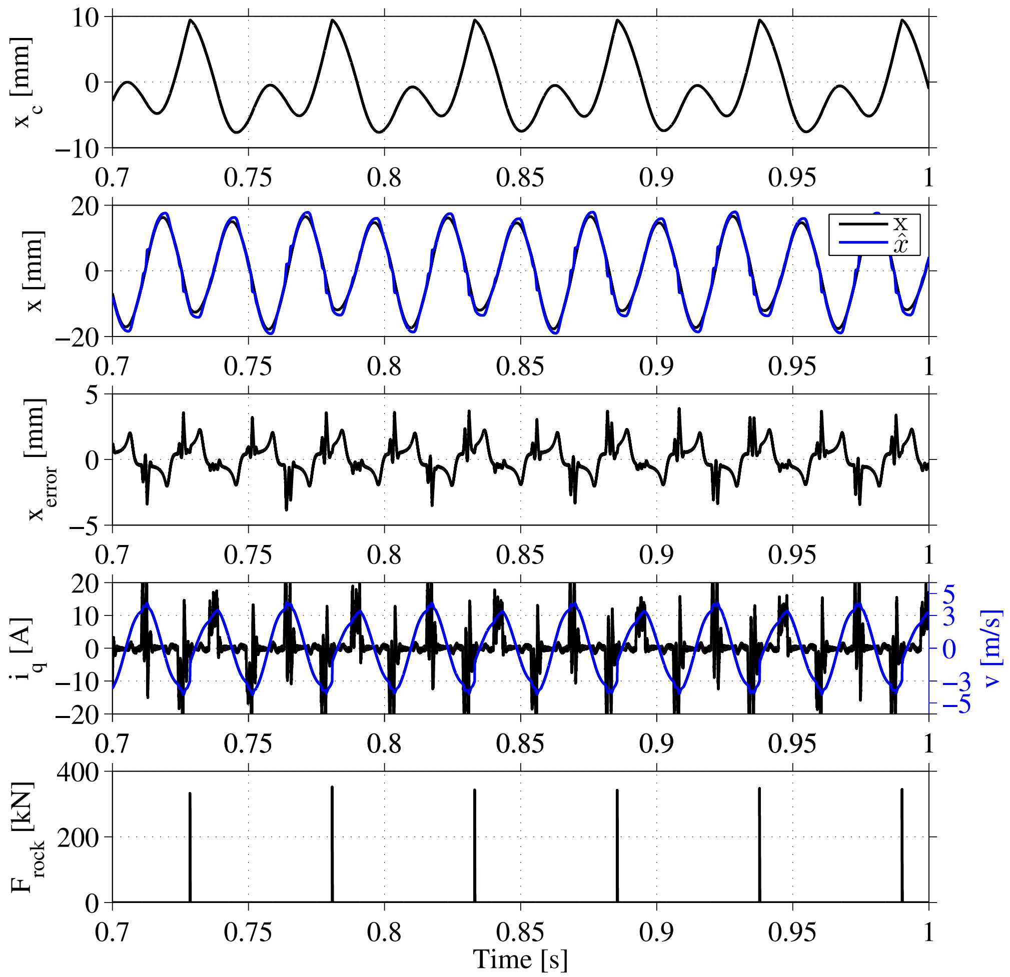


**Figure 6.10:** Behavior of complete system with oscillation control and SCVM. The control parameters are selected as $P$ = 400 Ns/m, $limit$ = 5 mm and $F_{WOB}$ = 200 N. The parameters for the SCVM are selected as $\alpha_0$ = 1000 and $\lambda$ = 2. 10% measurement noise added. Parameter estimations, $\Psi$=0.8$\hat{\Psi}$, $L$=0.8$\hat{L}$, $R$=0.8$\hat{R}$.

6.13 it can be concluded that the amplitude of the injected signal is important to the performance of this observer. Unless the application is very sensitive to force ripple it is recommended to use a high amplitude of the injected signal.

The bandwidth of the PLL determines how fast oscillations that can be tracked with the observer. A simulation was made with $U_h$=80 V where the oscillation frequency is increased by increasing the stiffness of the springs. In Figure 6.14a the maximum frequency that the observer is able to track when the Resonator is moved without hitting the rock is seen for certain bandwidths. In Figure 6.14b the maximum amount of noise in the current measurement that the observer is able

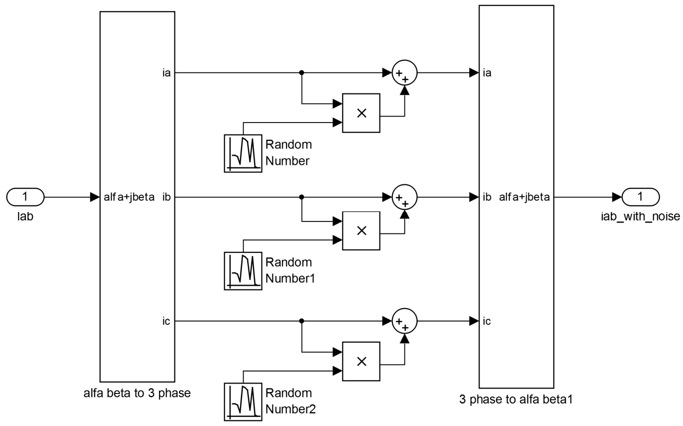


**Figure 6.11:** Block diagram used to add noise to the phase current measurement.

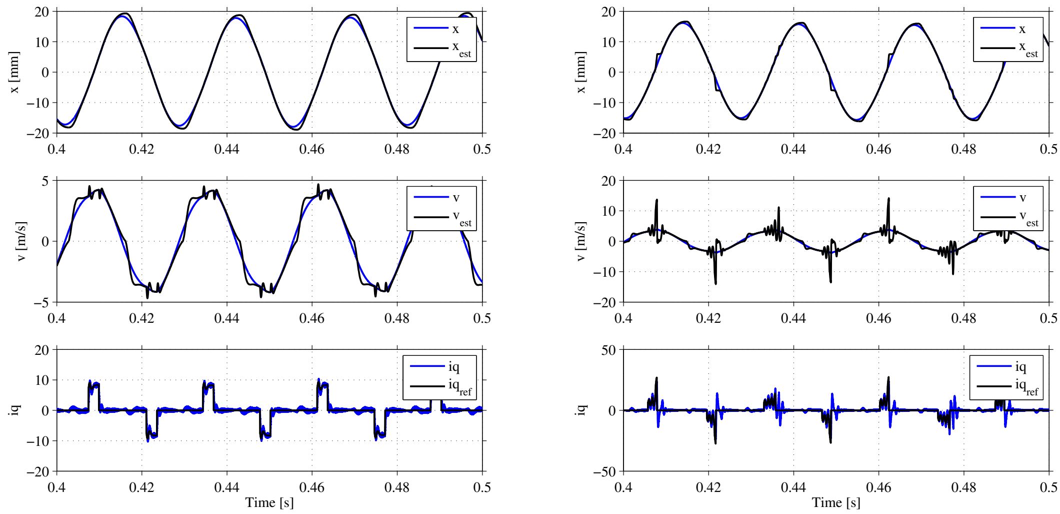


**(a)** Behavior with $\lambda$=2, $P$ = 300 Ns/m, $limit$ = 5 mm.

**(b)** Behavior with $\lambda$=5, $P$ = 300 Ns/m, $limit$ = 5 mm.

**Figure 6.12:** Sensitivity against current derivatives for two different values of the leakage term, $\lambda$, in the SCVM.

to handle is seen for different PLL bandwidths. Higher bandwidth means that the observer is more sensitive to measurement noise. By comparing Figure 6.14a and Figure 6.14b it can be concluded that for a system with fast oscillations it is crucial with good current measurement with low noise level. Otherwise the signal injection technique will not work.

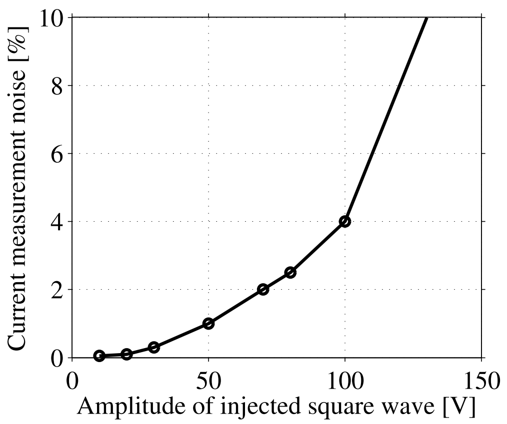


(a) Current measurement noise that the observer is able to handle with different amplitude of the injected signal.

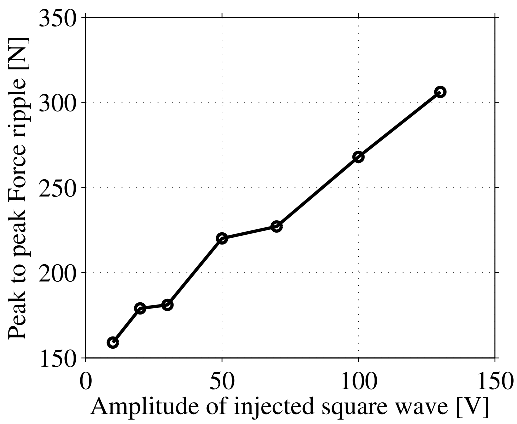


(b) Peak to peak ripple in the force generation with different amplitude of the injected signal.

**Figure 6.13:** Ability to handle noise and force ripple for increasing amplitude of injected signal. PLL bandwidth, $\rho$ is 500 rad/s.

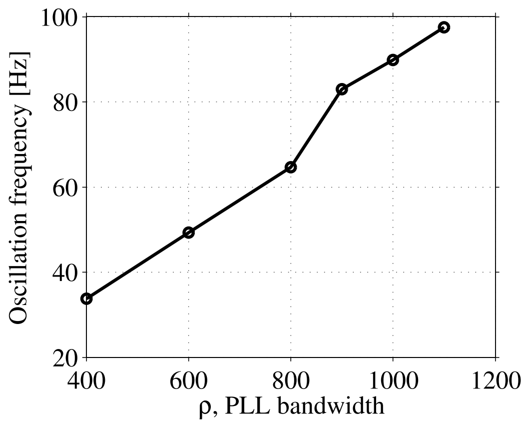


(a) Oscillation frequency that the observer able to track with different bandwidths, $\rho$.

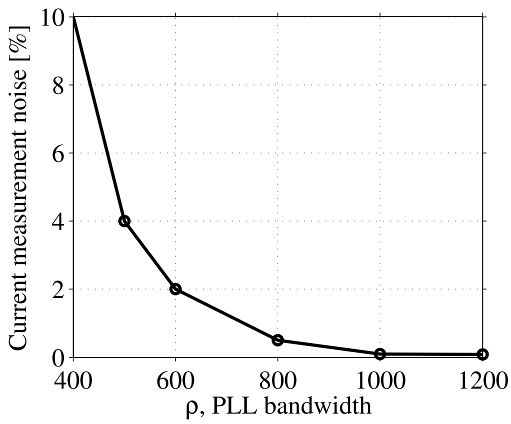


(b) Current measurement noise that the observer is able to handle with different bandwidths, $\rho$.

**Figure 6.14:** Ability to handle noise and ability to track fast oscillations for different bandwidths, $\rho$. Amplitude of injected voltage is $U_h$=80 V.

In Figure 6.15 the Resonator is simulated with estimated relative position and speed with the Square Wave Injection technique in an ideal case without measurement noise and parameter errors. The parameters in the control system are selected as $P = 400$ Ns/m, $limit = 7$ mm and $F_{WOB} = 200$ N and the parameters in the observer as $U_h$=80 V and $\rho$=600 rad/s. It can be seen that the Resonator behaves similarly to the case with ideal measurements of the relative position and speed, seen in Figure 6.6. A difference is that the q-current is applied a bit later than in the ideal case. This results in an impact force to the rock of only 364 kN which is smaller than in the ideal case, even if the controller limit was incresed. The reason to why the q-current is applied late is that the maximum position error in the estimation is at the time instant just before the q-current is applied.

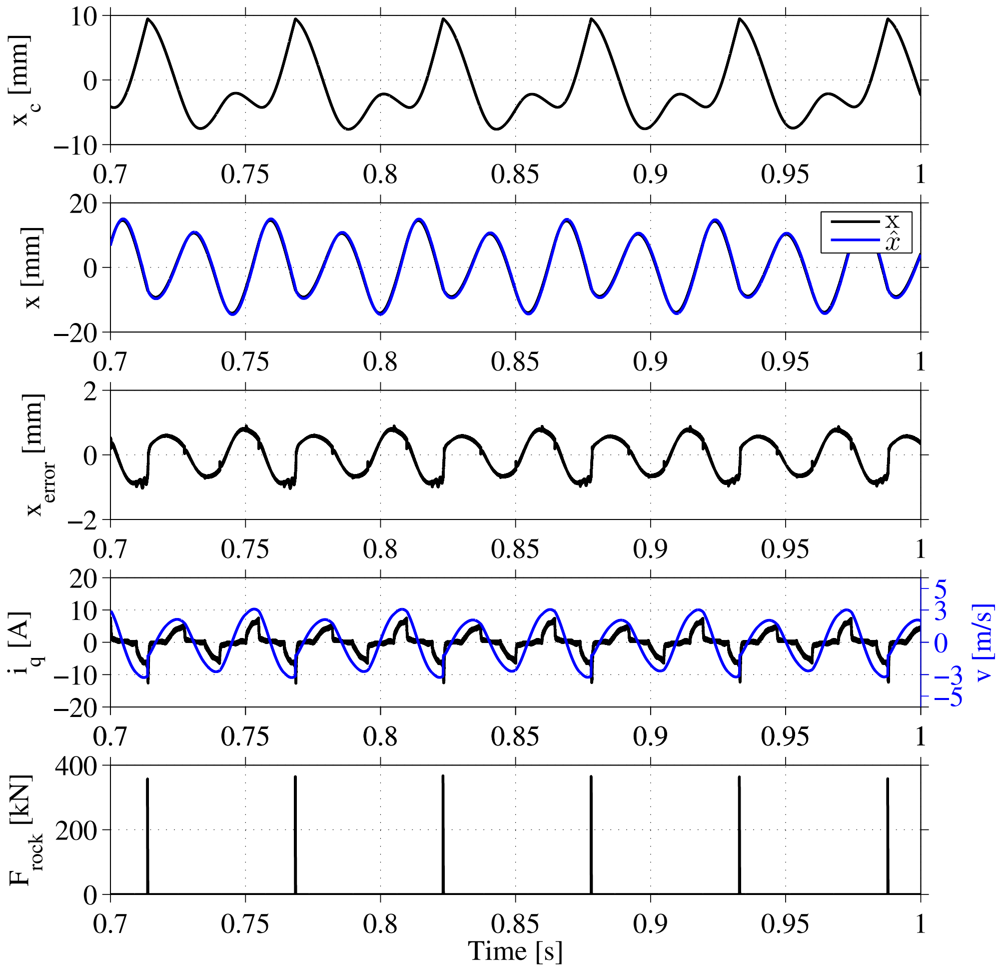


**Figure 6.15:** Behavior of complete system with oscillation control and square wave injection. The control parameters are selected as $P = 400$ Ns/m, $limit = 7$ mm and $F_{WOB} = 200$ N. The parameters for the square wave are selected as $\rho$=600 rad/s and $U_h$=80 V.

As concluded in Section 5.2.1, the Square Wave Injection technique is insensitive to parameter errors but sensitive to measurement noise. In Figure 6.16 the Square Wave Injection technique is simulated with a current measurement noise of 0.2%. The low amount of noise is needed since the method is even more sensitive to measurement noise when the Resonator is hitting the rock than it is when the Resonator is moving freely. It can be seen that the the estimation is poorest when the current is high. This is since the noise is 0.2% of the current value which means that it is high noise when the current is high. It is also seen that the largest estimation error is almost 3.8 times larger than without measurement noise and that the impact force to the rock is reduced to 350 kN.

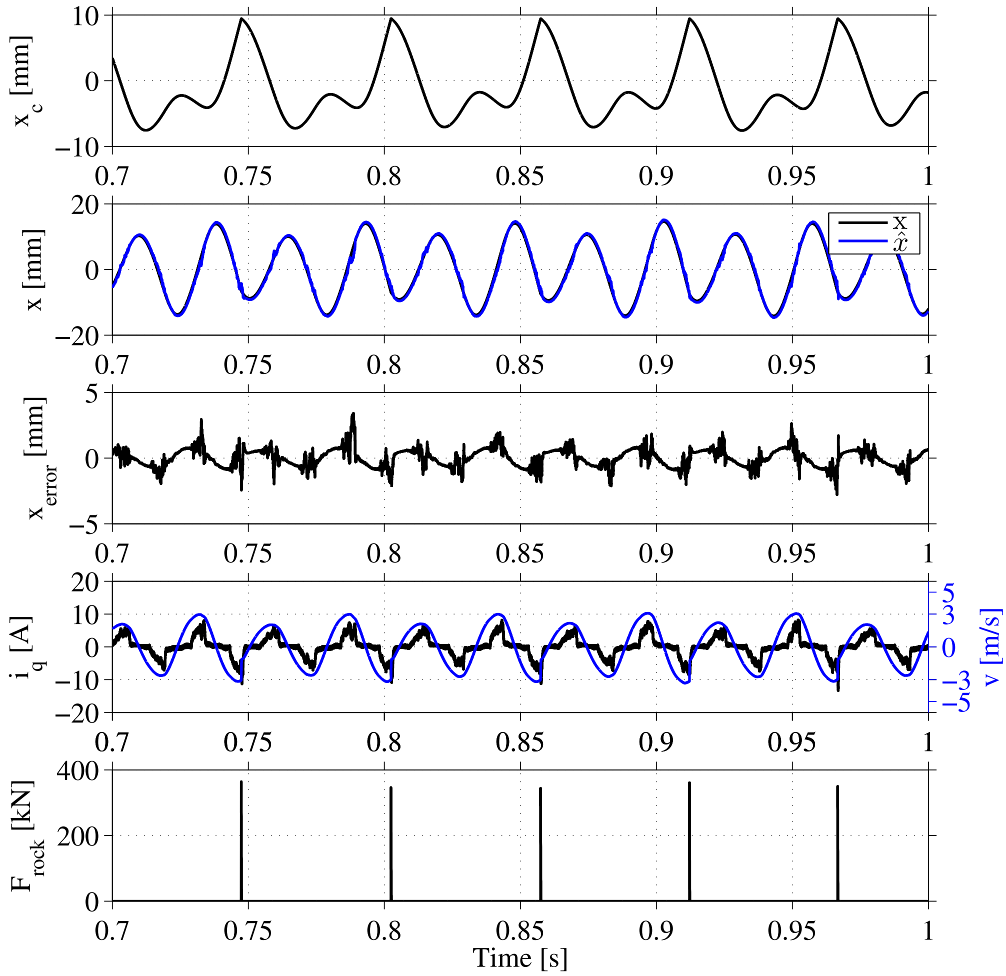


**Figure 6.16:** Behavior of complete system with oscillation control and square wave injection. The control parameters are selected as $P = 400$ Ns/m, $limit = 7$ mm and $F_{WOB} = 200$ N. The parameters for the square wave are selected as $\rho$=600 rad/s and $U_h$=80 V. Current measurement noise of 0.2% added.

# 7

# Conclusion and future work

## 7.1 Conclusion

In this thesis a control strategy for a percussive drill driven by a TLPMSM has been presented. The control strategy is based on a standard vector controller for the stator current and an outer proportional controller with positive feedback for the oscillations. The outer controller has particularly good properties for the application. The first important property is that it only demands a current when the TLPMSM has a relative speed between the rotor and stator and therefore is able to give an output power. When the relative speed is zero the TLPMSM is unable to produce any output power and then the current reference to the current controller is also zero. This prevents unnecessary copper losses.

The second property is even more important than the first. The outer controller controls the oscillations of the mechanical system without any information about the process parameters or a model of the rock. This is very useful since it is very difficult to make accurate models of rocks. Furthermore the mechanical system is always oscillated at its resonance frequency. Since the resonator is oscillated at the higher of its two resonance frequencies the piston and the casing are oscillated completely out of phase. This means that the relative motion between the piston and the casing and therefore also the back emf have a maximum which means that the current, for a fixed voltage, has a minimum. This reduce the amount of copper losses. It is shown that the relative position between piston and casing oscillates twice for each time the casing strikes the rock surface. In the simulated scenario, the impact force from the casing to the rock can reach 645 kN with an oscillation frequency of 38 Hz. To increase the oscillation frequency the gas spring pressure need to be increased.

In Chapter 5, two different strategies for making the control system sensorless are presented. The first strategy is a Statically Compensated Voltage Model and the second strategy is a technique denoted Square wave injection. Both techniques are working in the application but they have different advantages and disadvantages. It is shown that the SCVM is insensitive to measurement noise since 10 % noise could be added to the current measurement without any trouble. It is also shown that it is dependent on good parameter estimation, especially for the rotor flux. An error in the parameter estimations leads to a lowering of the impact force from the casing to the rock from 417 kN per hit to 343 kN per hit.

For Square wave injection it is the opposite. It is sensitive to measurement noise since only 0.2 % current measurement noise could be added without that the estimation stopped working. If the oscillation frequency is increased the noise level need to be even lower. However, it is not dependent on parameter estimations since process parameters are almost not used.

When each estimation techniques is simulated without measurement noise the square wave injection technique gives a lower maximum position estimaton error than the SCVM, 0.82 mm versus 1.64 mm. But for the square wave injection technique the position estimation error is high at the instant when the current is applied. Since the force generating current is erronously applied an impact force from the casing to rock of 364 kN is reached and this is lower compared to the impact force of 417 kN when the SCVM is used.

It is recommended to use SCVM for this application. The SCVM can be used in a larger range of oscillation frequencies for the mechanical system and is more robust against non-ideal conditions.

## 7.2 Future work

The TLPMSM was not assembled before the deadline of this work and therefore it was not possible to implement the proposed control strategy. Before the strategy is implemented it would also be preferable to measure all parameters of the machine to make the simulations as realistic as possible. Some of the parameters used in this work are selected to be reasonable since they were not completely determined before this work was finished.

How the closed loop controller parameters ($P$, *limit* and $F_{WOB}$) should be selected have not been fully examined. This should be investigated together with a more accurate rock model and eventually by experiments.

# Bibliography


[1] Core Writing Team, R. Pachauri, A. Reisinger, Contribution of Working Groups I, II and III to the Fourth Assessment Report of the Intergovernmental Panel on Climate Change, Tech. rep., IPCC, Geneva, Switzerland (2007).

[2] Enerdata, Total energy consumption in *Global Energy Statistical Yearbook 2013*, `http://yearbook.enerdata.net/` (January 2014).

[3] G. Nygaard, H. Gjeraldstveit, O. Skjæveland, Evaluation of automated drilling technologies developed for petroleum drilling and their potential when drilling geothermal wells, in: World Geothermal Congress, 2010.

[4] G. Samuel, Percussion drilling...is it a lost technique? a review, in: Permian Basin Oil and Gas Recovery Conference, 1996.

[5] S. Zhang, Percussive drilling application of translational motion permanent magnet machine, Tech. rep., Department of Electric Power Engineering, NTNU, Norway (2012).

[6] R. B. Ummaneni, R. Nilssen, J. Brennvall, Force analysis in design of high power linear permanent magnet actuator with gas springs in drilling applications, in: Electric Machines & Drives Conference, 2007.

[7] E. Hoff, J. E. Brennvall, R. Nilssen, L. Norum, High power linear electric machine-made possible by gas springs, Tech. rep., Norwegian University of Science and Technology, Department of Power Electronics (June 2004).

[8] R. B. Ummaneni, C. Jaillot, R. Nilssen, J. E. Brennvall, Experimental characterisation of linear permanent magnet actuator with gas springs, Electric Machines and Drives Conference (2009) 369–372.

[9] S. Zhang, L. Norum, R. Nilssen, Oscillatory motion application of tubular linear permanent magnet machine, IECON '09. 35th Annual Conference of IEEE (2009) 1223–1227.

[10] A. Bostad, Description and analysis of a resonating free-piston tubular permanent magnet linear machine, suitable for exploring the effects of increasing frequency in hammer drilling, Master thesis, Norwegian University of Life Sciences, Ås, Norway (October 2011).

[11] S. Zhang, L. Norum, R. Nilssen, Variable voltage variable frequency control of tubular linear permanent magnet synchronous machine for drilling applications, XIX International Conference on Electrical Machines (ICEM) (2010) 1–5.

[12] M. G. D. D. Y. Melamed, A. Kiselev, J. Blacis, Hydraulic hammer drilling technology:developments and capabilities,, Los Alamos National Lab, W-7405-ENG-36 (1996).

[13] R. Bekken, Experimental testing of a tubular linear permanent magnet machine for percussion drilling in hard rocks, Master thesis, NTNU, Norway (2011).

[14] E. B. Cole, Theory of Vibrations for Engineers, 4th Edition, Crosby Lockwood & Son Ltd., 1961.

[15] R. A. Serway, J. W. Jewett, Physics for Scientists and Engineers, 9th Edition, Brooks/Cole, 2013.

[16] R. R. Craig, A. J. Kurdila, Fundamentals of Structural Dynamics, 2nd Edition, John Wiley & Sons Inc, 2006.

[17] L. Harnefors, Control of variable-speed drives, Tech. rep., Department of Electrics, Mälardalen College University (2002).

[18] P. H. Tran, Matlab/simulink implementation and analysis of three pulse-width-modulation (pwm) techniques, Master thesis, Boise State University (2012).

[19] G. J. V. Wylen, R. E. Sonntag, Fundamentals of Classical Thermodynamics, 4th Edition, John Wiley & Sons Inc, 1994.

[20] P. Ponomarev, Control of permanent magnet linear synchronous motor in motion control applications, Master thesis, Lappeenranta University of Technology, Finland (2009).

[21] S. D. B. M. S. Sazidy, D. G. Rideout, F. Arvani, Modelling percussive drilling performance uding simulated visco-elasto -plastic rock medium, Tech. rep., Memorial University, St.John's, NL,Canada (2010).

[22] A. D. Batako, V. I. Babitsky, N. A. Halliwell, Modelling of vibro-impact penetration of self – exciting percussive-rotary drill bit, Journal of Sound and Vibration (271) (2004) 209–225.

[23] E. L. Chiang, D. A. Elias, A 3d fem methodology for simulating the impact in rock-drilling hammers, International Journal of Rock Mechanics & Mining Sciences (45) (2008) 701–711.

[24] S. Kim, J.-I. Ha, S.-K. Sul, Pwm switching frequency signal injection sensorless method in ipmsm, IEEE Transactions on Industry Applications 48 (5) (2012) 1576–1587.

[25] M. Jansson, L. Harnefors, O. Wallmark, M. Leksell, Synchronization at startup and stable rotation reversal of sensorless nonsalient pmsm drives, IEEE Transactions on Industrial Electronics 53 (2) (2006) 379–387.

[26] A. R. Setty, S. Wekhande, K. Chatterjee, Comparison of high frequency signal injection techniques for rotor position estimation at low speed to standstill of pmsm, Power Electronics (IICPE) (2012) 1– 6.

[27] P. L. Jansen, R. D. Lorenz, Transducerless position and velocity estimation in induction and salient ac machines, Industry Applications Society Annual Meeting 1 (1994) 488– 495.

[28] Y. doo Yoon, S. ki Sul, S. Morimoto, K. Ide, High bandwidth sensorless algorithm for ac machines based on square-wave type voltage injection, Energy Conversion Congress and Exposition (ECCE (2009) 2123– 2130.

[29] L. Harnefors, H.-P. Nee, A general algorithm for speed and postition estimation of ac motors, IEEE Transactions on Industrial Electronics 47 (1) (2000) 77–83.